Subsurface structure and stratigraphy of the northwest end of the Turkana Basin, Northern Kenya Rift, as revealed by magnetotellurics and gravity joint inversion,

Yassine Abdelfettah, Jean-Jacques Tiercelin, Pascal Tarits, Sophie Hautot, Marcia Maia, Peter Thuo

Accepted Manuscript

Subsurface structure and stratigraphy of the northwest end of the Turkana Basin, Northern Kenya Rift, as revealed by magnetotellurics and gravity joint inversion

Yassine Abdelfettah, Jean-Jacques Tiercelin, Pascal Tarits, Sophie Hautot, Marcia Maia, Peter Thuo

PII: S1464-343X(16)30093-0

DOI: 10.1016/j.jafrearsci.2016.03.008

Reference: AES 2523

To appear in: *Journal of African Earth Sciences*

Received Date: 2 August 2014

Revised Date: 13 March 2016

Accepted Date: 14 March 2016

Please cite this article as: Abdelfettah, Y., Tiercelin, J.-J., Tarits, P., Hautot, S., Maia, M., Thuo, P., Subsurface structure and stratigraphy of the northwest end of the Turkana Basin, Northern Kenya Rift, as revealed by magnetotellurics and gravity joint inversion, *Journal of African Earth Sciences* (2016), doi: 10.1016/j.jafrearsci.2016.03.008.

Subsurface structure and stratigraphy of the northwest end of the Turkana Basin, Northern Kenya Rift, as revealed by magnetotellurics and gravity joint inversion

Yassine Abdelfettah[a, b,c,*], Jean-Jacques Tiercelin[d], Pascal Tarits[b], Sophie Hautot[e], Marcia Maia[b], Peter Thuo[f, b]

[a] *Institut de Physique du Globe de Strasbourg, CNRS UMR7516, University of Strasbourg, Strasbourg, France*

[b] *UMR CNRS 6538 Domaines Océaniques, Institut Universitaire Européen de la Mer, Université de Bretagne occidentale, 29280 Plouzané, France*

[c] *Institut für Nukleare Entsorgung INE, Karlsruher Institut für Technologie (KIT), Karlsruher, Germany*

[d] *UMR CNRS 6118 Géosciences Rennes, Université de Rennes 1, Campus de Beaulieu, 35042 Rennes Cedex, France*

[e] *IMAGIR Sarl, 38 Rue Sevellec, 29200 Brest, France*

[f] *ERHC Energy Kenya Limited, Block D, Unit 1A, 3rd Floor, Sameer Business Park, Mombasa Road, P.O. Box 6008-00100 Nairobi, Kenya*

ABSTRACT

In order to understand the subsurface stratigraphy and structure of the northwest end of the Turkana Basin, Northern Kenya Rift, we used 2-D joint inversion of magnetotelluric (MT) and gravity data acquired along 3 profiles perpendicular to the main Murua Rith-Lapur Rift Border Fault. The regional geology is characterized by a basement of Precambrian age overlain by a ≤500-m thick sandstone formation named the Lapur

Sandstone of upper Cretaceous-lower Eocene in age, covered by thick rhyolitic and basaltic lavas of late Eocene-middle Miocene age, known as the “Turkana Volcanics”. Final interpretation of the resistivity and density models, until 5 km depth, obtained by the joint inversion approach confirms the previous general knowledge about the half-graben geometry of the northern part of the Turkana Basin. The main Murua Rith-Lapur Rift Border Fault is well identified by both gravity and MT. At least, two other important secondary faults without surface expression are also identified. A new small half-graben basin, named the Kachoda Basin, parallel to the main Turkana Basin and filled by 1.5 km of sediments, has been also characterized. This study also highlights strong thickness variations of the three main geological units that could be expected in the subsurface of the Turkana Basin. For example, the sedimentary Nachukui and Kibish Formations reach up to >3 km in thickness at the eastern end of the north and central profiles. Lateral variations of the topography of the Precambrian basement are also evidenced. Conceptual geological models, which result from the combination of the obtained density and resistivity models as well as from geological and reflection seismic data, are proposed. In such an area of intensive and promising oil exploration, these models are essential in terms of identification of reservoirs, source rocks and trapping mechanisms.

Keywords:

Northern Kenya Rift, Turkana Basin, Kachoda Basin, Lapur Sandstone, “Turkana Volcanics”, Sub-basalt imaging, magnetotelluric, gravity, joint inversion.

* **Corresponding author**. Tel.: +33 (0) 3 68 85 00 34

E-mail addresses: yassine.abdelfettah@unistra.fr (Y. Abdelfettah), riftman@orange.fr (J.-J. Tiercelin), tarits@univ-brest.fr (P. Tarits), sophie.hautot@imagir.eu (S. Hautot), marcia@univ-brest.fr (M. Maia), pthuo@erhc.com (P. Thuo)

1. Introduction

The north-western part of the Kenya territory is characterized by a wide NW-SE oriented tectonic depression known as the Turkana Depression, located immediately to the southeast of the oil-rich rift basins of southern Sudan (Fig. 1a). This region has been the subject of a major interest for possible commercial hydrocarbon potential (Morley, 1999; Wescott et al., 1999; Tiercelin et al., 2004, 2012b). In the north-western part of the Turkana Depression near the borders of South Sudan, Uganda and Ethiopia, gravity data acquired in the 80s by the Amoco Kenya Petroleum Company (AKPC) revealed wide elongate anomalies suggesting the presence at depth of two deep, N-S oriented sedimentary basins named the Lotikipi Basin to the west, and the Gatome Basin to the east (Wescott et al., 1999) (Fig. 1a). Because of insufficient geophysical data and the lack of exploration wells, the stratigraphy of these basins remained largely unknown. Very little seismic reflection data was acquired in this area by AKPC (e.g. Wescott et al., 1999) and it showed very low vertical resolution caused by the presence in the shallow subsurface of a 3.5 km thick pile of basaltic and rhyolitic lavas of Late Eocene-Middle Miocene age known as the “Turkana Volcanics” (Bellieni et al., 1981; Zanettin et al., 1983; Morley et al., 1999; Tiercelin et al., 2012). In the eastern part of the Turkana Depression, Project PROBE (Dunkelman et al., 1988, 1989) and AKPC (e.g., Morley et al., 1992; Wescott et al., 1999) conducted intensive land and offshore Lake Turkana reflection seismic campaigns that aimed at understanding

the subsurface geology in areas with poor surface outcrop conditions. Interpretation of these data allowed for the determination of the deep structure and sedimentary infill of several N-S-trending half-grabens ranging in age from Paleogene to Plio-Pleistocene, known as the Lokichar (North and South), North Kerio, and Turkana Basins, respectively (Morley et al., 1999; Tiercelin et al., 2004; Talbot et al., 2004) (Fig. 1a). The Lokichar and Turkana Basins have been tested during the 90s by two deep exploration wells, operated by Shell Exploration and Production Kenya B.V.: the Loperot-1 well drilled in the Lokichar Basin, and the Eliye Springs-1 well drilled in the Turkana Basin (Fig. 1a). These two wells confirmed the existence of thick alternating packages of fluvial, fluvio-deltaic and lacustrine sediments, of Eocene-Middle Miocene age for the Lokichar Basin, and Plio-Pleistocene age for the Turkana Basin (Morley et al., 1992, 1999). The Loperot-1 well demonstrated the presence of thick, organic-rich shales and oil shows in sandstone units (Wescott et al., 1999). In the last 5 years, more than ten exploration wells have been drilled by a group of oil companies (Tullow Oil and Africa Oil Corp.) in the South Lokichar Basin. All these wells revealed the presence of a large number of net oil pays in two main high quality reservoir horizons, known as the Lokone Sandstone and the Auwerwer Sandstone (Africa Oil Corporation, 2011, 2014) (Fig. 1a).

In this work, we present the results of an MT and gravity joint inversion survey devoted to understand the stratigraphy and structure of subsurface terrains of the northwest end of the Turkana Basin, a sensitive area where outcrop data are limited and where seismic studies are either absent or encountered a sub-basalt imaging problem and are therefore unable to bring accurate subsurface information (Fig. 1a and b).

Figure 1

2. Geological setting

The roughly N-S-oriented Turkana Basin occupies the central-eastern part of the Turkana Depression between latitudes 4° and 4.5° N, and hosts the present-day Lake Turkana, which is the largest water body of the Eastern Branch of the East African Rift System (Fig. 1a and c). The Turkana Basin started to form around Middle Miocene (15-10 Ma) (Dunkelman et al., 1988, 1989; Morley et al., 1992; Dunkley et al., 1993; Morley et al., 1999). The northern half of the basin reveals a typical east-facing half-graben structure bounded by a set of N-S oriented normal faults morphologically marked by the main Murua Rith-Lapur (MRL) Border Fault escarpment (Fig. 2a). Geologically, the MRL Border Fault footwall and hanging wall displays a simple stratigraphic succession with, unconformable overlying a Precambrian basement mainly formed by migmatites and amphibolites (Walsh and Dodson, 1969) (Figs. 2a-c and 3a), an up to 500-m thick accumulation of conglomerates, sandstones, siltstones and mudstones named the Lapur Sandstone (Figs. 2a and b and 3a and b), thinning and disappearing toward the north at about 4.45° N and toward the south at Keniroliom (04° 11’10’’ N, 35° 49’ 41’’ E) (Thuo, 2009; Tiercelin et al., 2012) (Fig. 1d). Overlying the Lapur Sandstone are the “Turkana Volcanics” that widely outcrop to the west, in the Gatome and Lotikipi regions, where they reach a maximum thickness of 3.5 km (Bellieni et al., 1981; Zanettin et al., 1983; Tiercelin et al., 2012a) (Figs. 1a, 2 and 3c). To the immediate west of the MRL escarpment is a small roughly N-S oriented, ~15 km wide, flat-bottomed valley bounded on both sides by basalts and rhyolites belonging to the “Turkana Volcanics”, forming the eastern faulted flank of the Gatome Basin. This valley, known as the Kachoda Valley, opens towards the north into the Sanderson’s

Gulf and the Todenyang Plain to the immediate west of the Omo River delta (Fig. 1c and d). Alluvial-type sediments of unknown age and thickness characterize the surface of this valley.

Figures 2, 3 and 4

To the east of the MRL Border Fault, the subsurface stratigraphy of the MRL hanging wall can be deduced from the interpretation of one W-E oriented, onshore reflection seismic line (TVK-10) acquired by AKPC in 1985 at 4.13°N, between the MRL escarpment and the Lake Turkana shoreline (Figs. 1d and 2c). Wescott and co-workers interpret this seismic line as showing a thick (up to 2 sec TWTT) pile of Late Miocene-Pliocene sedimentary rocks, conformably overlying the top of Middle Miocene volcanics belonging to the "Turkana Volcanics" unit (Wescott et al., 1999; Fig. 2). A recent interpretation of this TVK-10 seismic line (Tiercelin et al., 2012a) (Fig. 4) suggests the presence in the hanging wall of the MRL Border Fault, below the ''Turkana Volcanics'', of a 300-m thick sedimentary package that could be interpreted as the Lapur Sandstone. The ''Turkana Volcanics'' are in turn overlain by thick (1.5 sec TWTT) sediments forming the uppermost part of the infill of the Turkana Basin. Only the upper sedimentary deposits that characterize the hanging wall of the MRL Border Fault are known at the outcrop level. These deposits correspond to a southwest-dipping pile of fluvio-lacustrine sediments of Plio-Pleistocene age (dated between 4.2 and 0.7 Ma) known as the Nachukui Formation (Feibel et al., 1989) (Fig. 3d). This ~740-m thick sediment accumulation is overlain at the northern end of the Turkana Basin by upper Pleistocene to Holocene sediments of fluvio-deltaic type, that possibly belong to the 100-m thick Kibish Formation, dated at about 0.2 Ma at its base

and outcropping largely at about 5° 25'N along the Omo River, nearby the Nkalabong Range (Brown and McDougall, 2011) (Fig. 1c). Offshore seismic reflection data obtained by the PROBE Project indicated for the Turkana Basin a 4-km thick sedimentary infill immediately overlying the thick pile of the "Turkana Volcanics" (Dunkelman et al., 1988, 1989). Near the southern end of the Turkana Basin, the Eliye Springs-1 exploration well penetrated 2964 m of fluvio-lacustrine sands and shales similar to surface outcrops lying to the north and possibly belonging to the Nachukui Formation (Fig. 1c).

3. Magnetotelluric and gravity surveys

The study area is mainly located on the western faulted side of the northern part of the Turkana Basin, between latitudes 4.1305 and 4.4001° N and longitudes 35.5890 and 35.9280° E in WGS84 system (Fig. 1). Magnetotelluric and gravity data as well as complementary field observations were acquired during one field campaign conducted in August 2006 in cooperation with teams from two Kenyan companies, the Kenya Electricity Generating Company (KenGen) and the National Oil Corporation of Kenya (NOCK). We carried out a total of 27 magnetotelluric soundings along three W-E oriented profiles, almost perpendicular to the main N-S geological strike direction illustrated by the MRL Border Fault (Fig. 1b). The southern profile (P1) was superimposed on the trace of the W-E oriented TVK-10 seismic reflection line whose track was still clearly visible in the field (Fig. 1b and d and 2). The median profile (P2) followed the car track coming from the western shoreline of Lake Turkana through the Lowarengak village then the Lokitaung Gorge, crossing the MRL escarpment up to the township of Lokitaung (Fig. 1b and d and 2). This profile extended 15 km further to the west, following a track running almost E-W, crossing through the Kachoda Valley (Fig. 1b and d and 2). To the north, the field survey

was limited at latitude 4.40° N because of the bad security conditions nearby the Sudan and Ethiopia borders. The northern profile (P3) extended toward the east in the area of the Lapur Peak, from the trace of the MRL Border Fault up to the shoreline of Lake Turkana (Figs. 1a, d and 2).

The MT sites were spaced at an average distance of about 1.5 km, with the exception of two stations on the median profile (between station 22 and station 23, and between station 24 and station 10 situated in the narrow and deep Lokitaung Gorge (Fig. 1b). Here, the distance between the two stations was much larger as it was not always easy to find a suitable place to record the electrical component. Data were acquired using a Phoenix system provided by KenGen (Fig. 5c-e). The electric and magnetic fields were recorded in N-S and E-W perpendicular directions.

The gravity measurements were made using a Lacoste-Romberg gravimeter also provided by KenGen (Fig. 5a and b). Gravity was measured at 243 points along the three MT profiles (Fig. 1b). The measurement points were spaced at an average distance of 250 m, with the exception of the Lokitaung Gorge where this distance was larger as a consequence of the morphology of the gorge. Nevertheless, its spatial resolution remained greater than the MT sites. The quality of both MT and gravity data was relatively good and the MT data showed little noise (see Fig. 6).

Figures 5 and 6

4. Geophysical data processing

4.1 MT processing

The magnetic and electric time series were processed robustly with the algorithm of Chave and Thomson (2004), covering the period range 0.02–450 s. Because of difficult field conditions and no remote reference (Goubau et al., 1978), data were carefully edited

and only time series of good quality were processed, reducing the number of robust estimates and increasing some of the error bars (Fig. 6). Overall, MT transfer functions are of fair to good quality. The complex conjugate directions of the tensor were computed (Counil et al., 1986) to study the dimensionality of the data. Both electric and magnetic directions are similar, an indication of a weak effect of local 3-D heterogeneities. Electric directions for all sites are shown in Fig. 7 at two periods. In general, they indicate a rough N-S strike direction for the transverse electric TE mode (e.g., Parker, 2011) on the central profile, although directions may vary locally, particularly within the Lokitaung Gorge. These directions indicate therefore only approximately a true 2-D strike. Nevertheless, the 3-D modelling of the three profiles confirmed that a local 2-D approach is suitable for most of the sites for the first kilometres in the crust (Abdelfettah, 2009), with a main strike direction in agreement with the geological trend. The central profile has 2 stations (23 and 24) within the Lokitaung Gorge (Fig. 1b and d), 5 stations on the western side of the Turkana Basin (from west to east: 10, 11, 25, 26 and 27), and 5 stations in the Kachoda Valley (from west to east: 18, 19, 20, 21 and 22). Two stations, 22 and 23, show moderate static shift (Groom et al., 1989; McNiece and Jones, 2001) in the transverse magnetic, TM mode in relation with the topography that was accounted for in the 2D modelling. The other profiles are located on the western side only of the Turkana Basin, from the trace of the MRL Border Fault to the west up to the Lake Turkana shoreline to the east. Because of the high conductivity (1 Ω.m) of the sedimentary infill of the Turkana Basin, no significant topography effect was observed in the other stations of the three profiles. Details of the MT study and modelling can be found in Abdelfettah (2009).

Figures 7

4.2. Gravity processing

The first correction performed on the acquired gravity data is the instrumental drift. The second correction is the terrestrial tide, which is of small amplitude but was considered in order to make a complete data processing sequence. After these two corrections, the free air reduction was applied on the data to obtain the free air anomaly (Fig. 8), which is the final anomaly used for the inversion. Rather than calculating the complete Bouguer anomaly, we use the free air anomaly and included the topography (Fig. 1b) correction (plateau and terrain corrections) directly in the modelling process. The latter consists of reproducing the topography of the area and, calculating its gravity effect at the measurement sites using a digital terrain model (DTM) of the studied area (SRTM3, 2003). The average density of the topography terrains was estimated based on data from the literature (2,450 kg.m^{-3}), and adjusted such that the Bouguer anomaly was de-correlated from the topography. The density value taken into account in the calculation of the gravity effect of the terrains is 2,450 kg.m^{-3}. The gravity effect of Lake Turkana (water density 1,000 kg.m^{-3}) was also taken into account in the forward modelling.

Figure 8

5. Joint inversion formulation

5.1. MT and gravity inversion method

The forward solution for MT is obtained with a 2-D finite difference algorithm (Tarits, 1989). The objective function F(r) of MT combines the MT misfit and a regularisation term:

$$\boldsymbol{F(r) = \sum_{i=1}^{nst}\sum_{j=1}^{np}\left\{\left|\frac{Z_{ij}^{O\ TE} - Z_{ij}^{C}(r)^{TE}}{\sigma_{ij}^{TE}}\right|^2 + \left|\frac{Z_{ij}^{O\ TM} - Z_{ij}^{C}(r)^{TM}}{\sigma_{ij}^{TM}}\right|^2\right\} + \lambda_r S_r^2} \qquad \textbf{(1)}$$

where Z is the 2-D MT impedance. The indices O and C are respectively the observed

and calculated impedances for both transverse electric (TE) mode (the horizontal electric field parallel to the strike) and transverse magnetic (TM) mode (the horizontal magnetic field parallel to the strike) (e.g. Simpson et Bahr, 2005). The values nst and np are the number of sites and the number of periods respectively. The term σ is the standard deviation for each mode. The smoothness function S_r is defined by

$$\boldsymbol{S_r = \sum_{i=1}^{N-1} \sum_{j=i+1}^{N} \left(r_i - r_j\right)^2} \qquad \textbf{(2)}$$

where N is the number of parameters, r the log-resistivity, and λ_r is a damping coefficient. The 2-D model is bounded on both sides by one-dimensional (1-D) structures. The layered 1-D earth model is extended about 3-4 skin depth for the highest resistivity in both right and left sides to avoid the effect of our 2-D structures (e.g. Doucet et Pham, 1984).

The gravity model response is calculated at the earth surface from the gravity attraction generated by all rectangular prisms (e.g., Blakely, 1995). The objective function $F_G(d)$ for the gravity data is defined by

$$\boldsymbol{F_G(d) = \sum_{i=1}^{Ng} \left(\frac{g_i^O - g_i^C(d)}{\sigma_{g\ i}}\right)^2 + \lambda_r S_d^2} \qquad \textbf{(3)}$$

where N_g is the number of data points, σ_g is the standard deviation of measured gravity data. g^O and g^C are the observed and the computed gravity anomalies, respectively. The gravity smoothness function S_d is computed using Eq. 2 where the parameter r is now the density contrast.

5.2. Joint inversion formulation

Let a couple of model parameters *r* and *d*. We define a multiple objective function *Q(r,d)* of the form

$$\begin{cases} min\{Q(r,d) = F_{MT}(r) + F_G(d)\} \\ subject\ to\ d = \psi(r) \end{cases} \quad \textbf{(4)}$$

The function ψ is a condition function (CF) coupling the parameter r and d. The CF may be included in the inversion as a deterministic relationship between parameters (e.g., Tiberi et al., 2003) or a geometrical constraint (e.g., Gallardo et Meju, 2007). Here we investigate a solution based on a CF combining geometrical constraint and a relationship between the parameters r and d. We named this CF a geometrical condition function (GCF). We use the GCF to build the starting model $d_0=\psi(r_0)$ from a model r_0 obtained independently. This GCF assigns d_0 values according to a given rule in regions or domains defined by the geometrical features extracted from the model r_0. Once the inversion started, the parameters are free to vary within the fixed domains and no longer guided by that rule.

Figure 9

First we obtain a preliminary resistivity model (PRM) r_0. This was achieved with the minimisation of (Eq. 1). The geometrical features in model r_0, named domains, correspond to regions in the PRM where the resistivity values vary by less than one order of magnitude and to the regions delimited by strong resistivity contrasts. The density model d_0 was set constant in these domains and defined according to low (high) resistivity correspond to low (high) density. The extreme values of low and high density are defined from geological knowledge or previous studies in the same area and from the surrounding, for instance 2,750 $kg.m^{-3}$ for a Precambrian basement and 2,000 $kg.m^{-3}$ for Nachukui Formation. Then, the intermediate density values are obtained by linear relationship between density and $\log_{10}$ resistivity values. With this starting density model, the gravity data were introduced in the inversion algorithm and

the Eq. 4 is used for the total objective function.

The minimisation routine used to achieve this work is based on a steepest descent technique derived from Beiner (1970) (see also Fischer and Lequang, 1981) and based on downhill simplex method (e.g., Press et al., 1992) and therefore may only find a relative minimum of the objective function. The derivatives of the function are not calculated, hence the function itself is called and all differences in the parameters space are stored until the descent is found. The algorithm calls once the forward MT and gravity solutions each iteration.

We run the first stage of the inversion (stage 1). During the minimisation of Q(r, d), density values were free to change but the PRM domains defined above are still enforced, that is the density remains constant within the domains. Once a relative minimum for Q is found, the conditions on the density model are changed. The density values could vary within a domain where it was previously constant and a second minimization (stage 2) is carried out.

In practice, in our MT and gravity formulation, we adopt a common inversion grid based on 2-D prisms to run the joint inversion (Fig. 9). The MT inversion grid is defined on the basis of the data distribution and the frequency range (e.g., Fig. 9). The gravity inversion grid is mapped on the MT inversion grid. Hence there is the same number N of density cells and resistivity cells (Fig. 9). Aforementioned, we run the joint inversion in two steps. First, the density values were grouped into large homogeneous domains (piece-wise) defined by the PRM so that the number of density values sought is a small number (< 20 parameters) compared to N. The density values in this initial density model are determined by the GCF. Stage (1) constrains the gravity inversion with a fixed geometry obtained from the preliminary MT inversion.

In stage (2) we relax the constraint of fixed large domains of homogeneous density. We let the density value to evolve in all cells within the domains so the number of density values (N) required becomes equal to the number of resistivity values (N). This last step is important to check whether the density model obtained at stage 1 is robust, and to improve the final gravity and MT fits.

6. Density and resistivity models

Abdelfettah (2009) has tested the MT inversion and the MT-gravity joint inversion techniques on synthetic models and on real data. For the Turkana Basin study (Abdelfettah 2009), resistivity and density models obtained from the joint inversion for the three profiles are represented in Figs. 10, 11, 12 and 13 down to a depth of 5 km.

The resistivity models are characterized mainly by three major units (Figs. 10a, 11a, 12a and 13a).

- A shallow conductive unit with resistivity values, less than 10 Ω.m;
- Resistive units with resistivity values higher than 100 Ω.m;
- Between these two units, a third unit with intermediate resistivity values between 10 and 100 Ω.m (Figs. 10a, 11a, 12a and 13a).

Figures 10, 11, 12, 13

The density models obtained in this study (Figs. 10b, 11b, 12b and 13b) show that the central and southern profiles have similar characteristics (with Figs. 11a, 12a and 13a). In contrast, the northern profile (Fig. 10b) shows some differences in terms of thickness of the observed geological units compared to the southern profiles, especially in the eastern part near Lake Turkana shoreline. These differences may be partly attributed to the presence of a local three-dimensional heterogeneity located at depth between this profile and the central

profile as revealed by a complementary 3D MT inversion (Abdelfettah, 2009; Fig. 4.10). The central and southern profiles show a good correlation between the variation of resistivity and density values. Usually, a lower density corresponds to a conductive unit while a higher density corresponds to a resistive unit. The resistivity values and particularly high-density contrasts highlight the complex structures of the Turkana Basin and the Kachoda Valley, respectively.

7. Subsurface structure of the Turkana Basin

7.1. Northern profile (P3)

The resistivity model obtained for the northern profile (Fig. 10a) shows an upper limit (L1) between a very conductive geological unit (<10 Ω.m) and a more resistive zone where resistivity values vary between 10 and 50 Ω.m. This limit is located at a depth of 1.4-1.5 km on the western part of the profile, under station 13 near the trace of the MRL Border Fault. This layer may be interpreted as the base of the known sedimentary unit the Nachukui Formation and its upper Pleistocene-Holocene coverage (Kibish Formation) (McDougall et al., 2005). This result may confirm the presence in this northern part of the Turkana Basin of a more significant sediment thickness than the one observed further south (740 m for the Nachukui Formation). However the L1 limit is not well defined in the density model which shows significant lateral variations seemingly controlled by faults.

We seem to observe the signature of faults in both the density and resistivity models. The major MRL Border Fault to the west end has a surface expression and is clearly expressed in the density model (Fig 10b). Two secondary faults: the F0N Fault at the east of the profile between sites 13 and 14, and the F3N Fault between sites 16 and 17 seem identified in the resistivity model but are less clearly in the density model. The structures in the middle part of the profile in the density model could be interpreted as the signature of

faults: the F1N Fault between sites 14 and 15, and the F2N Fault between sites 15 and 16. The traces of these two last faults are not so clearly imaged in the resistivity model but seem constrained by the density distribution. The F0N and F3N faults as well as the F1N and F2N faults have no surface expression.

Towards the east, the limit (L1) appears at a shallow depth, 1.2-1.3 km under site 15, and reaches ~1 km depth midway between sites 16 and 17, at the eastern end of the profile when approaching the Lake Turkana shoreline. These variations in depth are also observed in the density model where the highest negative density contrasts thicken from East to West. This thickening is in agreement with the general dip to the west of the sedimentary beds of the Nachukui Formation as it is observed at the surface along the northwest shoreline of Lake Turkana. The fact that the resistivity distribution is not strongly marked by the FN1 and FN2 faults suggests that the material has no significant resistivity contrast.

At the eastern end of the profile, immediately east of the F3N, the (L1) limit is no longer visible, and the thickness of the identified sediments reaches a value of 2.5 km, but possibly higher. Another limit, named (L0), can be observed both in the density model and within the very conductive unit but poorly constrained by the data. If real, it could be interpreted as being the upper limit of a known large salt-water wedge (e.g. Johnson et al., 1987) associated to Lake Turkana (Fig.10).

A weakly defined second limit (L2) is suggested in the lower part of the fairly conductive package but again not well identified in the density model. Under site 13, (L2) occurs at a depth of ~2 km, and is found at a depth of ~1.8-1.9 km under site 16. To the east, (L2) is visible at a depth of ~1.4 km near the F3N Fault. From F3N toward the east, (L2) is no longer visible.

In terms of lithostratigraphy, the layer between L1 and L2 could be interpreted as the

volcanic pile known as “Turkana Volcanics”. At the western end of the profile, near the MRL Border Fault, this layer shows a thickness of about 0.6-0.7 km under site 13 that remains relatively constant toward the east. Then, from site 16, it decreases toward the east until crossing F3N, and reaches a thickness of ~0.4-0.5 km between sites 16 and 17. The high resistivity value and no density contrast between sites 16 and 17 suggest intrusion of volcanics in the sediments which are not outcropping probably because recovered by the recent Pleistocene-Holocene coverage.

At a greater depth (≥2 km), the model under station 13 and up to the western side of station 17 shows a high resistivity unit with values exceeding 100 Ω.m, excepted between sites 16 and 17 where the mean resistivity value is around 50 Ω.m. The top of this high resistivity unit corresponds to the limit (L2). Geologically, this unit would correspond to either the Lapur Sandstone or the Precambrian basement. The clear identification of the Lapur Sandstone, which is stratigraphically interbedded between the “Turkana Volcanics” and the Precambrian basement (Fig. 3c), is difficult because of the low resistivity contrast existing between the strongly consolidated sandstones and the overlying Precambrian basement (Fig. 3a), which both may have high resistivity values. In addition, the depth of investigation (>2 km) and the relatively weak thickness of the Lapur Sandstone in the area of the northern profile, evaluated at 100-120 m at the Lapur Peak (Tiercelin et al., 2012) make their detection even more challenging. Under the Lapur Sandstone and/or Precambrian basement, another limit (L3) can be identified. This limit separates a resistive part (that corresponds to the basement and/or the Lapur Sandstone) and a conductive part, which could correspond to a zone of intense fracturing to explain the increase of the conductivity values.

The density model (Fig. 10b) shows only some vertical variations comparable to the resistivity variations, which can relate to the presence of the MRL Border Fault and the

other secondary faults, F1N, F2N and F3N present in the central and eastern part of the profile. The upper limit of the LS and/or the Precambrian basement, marked by the (L2) boundary appears relatively flat between sites 13 and 16, whereas it shows a slight dip to the west between sites 16 and 17, delimited by the faults F2N and F3N. Immediately east of site 17, this limit disappears. The thickness of the Lapur Sandstone seems relatively constant (~100 m) from west to east, and does not exceed 120 m in the northern part, as observed in the Lapur Peak cliffs (Figs. 2 and 3).

To the east of F3N, under the site 17 and eastward (Fig. 10a), the (L1) and (L2) limits previously described are no longer visible. Very weak resistivity values (<10 Ω.m) can be found from the surface down to a depth of 5 km. The density contrast is negative and does not exceed 70 kg.m^{-3}. One sub-horizontal density contrast limit, named (L0), is identified at ~1 km depth and may represent the upper limit of a wide salt-water wedge (Fig. 10). Although the MT data have been processed in 2-D, the rapid change in structures from profile P3 to P2 and the absence of the limits (L1-L2/L3) under site 17 and eastward could suggest the resistivity model in P3 is biased by lateral 3-D variations in depth. In fact, the data do not exhibit strong 3-D distortion as revealed in Figure 7 and in the 3-D inversion presented in Abdelfettah (2009).

These high conductivity and negative density contrasts could be the result of the presence at the northwest end of the Turkana Basin of an important thickness (>2.5 km) of sediments belonging to the Plio-Pleistocene/Holocene Nachukui and Kibish Formations, or even older sediments. This thickness value is of the same order than the thicknesses observed on the PROBE seismic lines as well as on the Eliye Springs-1 well. This significant sediment thickness could be explained as resulting of a major subsidence associated to a high sedimentation rate along the F3N Fault, which thus could be considered as the main border fault of the Turkana Basin activated during at least the Pliocene and Pleistocene/Holocene

periods, compared with the main MRL Border Fault and the other secondary faults.

7.2. Central profile (P2)

The central profile crosses from the east the littoral/alluvial plain forming the western side of the Turkana Basin, then the MRL Border Fault escarpment and the Lapur Range through the Lokitaung Gorge, and ends to the west on the western side of the Kachoda Valley (Fig. 1).

The density and resistivity models presented in Fig. 11a and 11b show similar features mainly a horizontal contrast defining the (L1-L3) limits. One major discrepancy between density and resistivity models is around the depth of the limit (L2), which is imaged by MT but not well resolved by gravity. The resistivity model shows a clear contrast whereas the recovered density model is more homogeneous. Perhaps in this area, the "Turkana Volcanics" are less fractured as in the other places (in northern profile?).

At least three secondary faults can be identified in this model (Fig. 11). The major MRL Border Fault is clearly visible at the western end of the profile. Between sites 11 and 25, the F1C Fault, and between sites 25 and 26, the F2C Fault, are identified and interpreted as the cause of the down lift of the three geological units identified in this location. A third fault, named F3C, is visible between sites 26 and 27. The F2C and F3C Faults can be correlated with the F2N and F3N faults identified in the northern profile (Fig. 10).

The density model obtained for the Turkana Basin for the central profile (P2) (Fig. 11b) shows almost similar structures as those observed in the resistivity model (Fig. 11a). A negative density contrast ~200 kg.m^{-3} is visible in the eastern part from the surface down to ~0.9 km depth, and possibly represents the (L1) limit. The density values increase smoothly from this depth to reach a positive density contrast of ~200 kg.m^{-3} at a depth of 1-1.1 km at

the centre-east of the profile (under site 26). This limit could be attributed to the (L2) boundary. A negative density contrast of 50 kg.m^{-3} can also be observed under sites 10 and 11, that could correspond to a thin sedimentary layer (<150 m thick), the possible the (L1) limit. Below (L1), a positive density contrast of about 150 kg.m^{-3} is visible at a depth of ~1.2 km under site 11, and at ~1.7 km depth under site 10 (Fig. 11b). In terms of lithostratigraphy, the limit (L1) may correspond to the base of the Nachukui Formation at a depth of ~100-150 m under the sites 10 and 11, immediately east of MRL Border Fault (Fig. 11).

Four faults are well identified along the (P2) profile: the main MRL Border Fault, and three synthetic faults named F1C, F2C and F3C. At a distance of 7 km from the western end of the profile (between sites 11 and 25), the (L1) limit is found at a depth of ~0.5 km, immediately west of the F2C Fault. To the east and at a distance of ~5 km from the eastern end of the profile, the limit (L1) appears almost horizontal (under site 26) and reaches a depth of ~0.8 km immediately to the west of the F3C Fault. The (L2) limit, which is defined as the base of the "Turkana Volcanics", is identified below (L1) at a depth of ~1.2 km under site 26. It finally reaches a depth of ~2.2-2.3 km under site 27 near the Lake Turkana shoreline. The limit (L3) is partially visible below (L2), at the east end of the profile, at the depth of ~3.7-3.8 km under site 27.

The resistivity and density models obtained for this profile (Fig. 11) have different features in comparison to the northern profile. The conductive layer observed in the eastern half of the profile and interpreted as the Nachukui and Kibish Formations, is thinner than in the northern profile (1.3-1.4 km), (Fig. 11a). Under sites 10-11 and westward, this layer vanishes. Another difference with the northern profile can be observed at the eastern end of the central profile, from site 26 eastward to the lake shoreline (Fig. 11a), where the conductive layer continues monotonically toward the lake. Finally; the "Turkana

Volcanics" in P3 seem thicker in P2 with no clear evidence of the Lapur sandstone.

In some places, the intermediate density/resistivity values are not visible (e.g., Fig. 11). This behaviour could be explained partly by the fact that large cooling structures such as columnar jointing, colonnades and tores affect the basaltic flows of the "Turkana Volcanics" (Fig. 3d). Several metres or tens of metres wide dykes and thick sills also intrude the "Turkana Volcanics" pile (Fig. 3f). Several metres thick beds of strongly brecciated lavas also separate the main massive lava flows. Such types of structures may induce discontinuities within the pile of lavas that may explain the relatively low average resistivity values

7.3. Southern profile (P1)

The resistivity and density models for the southern profile and their structural interpretation are presented in Figure 12. They reveal again an upper conductive and low density layer, here about 2 km thick over a more resistive and denser medium. The resistivity and density contrast values are on average less than for profile P2. The signature of three faults may be identified along the profile: the MRL Border Fault at the western end of the profile, the F2S Fault at the centre of the profile under the sites 04 and 06, and the F3S fault near the eastern end of the profile between sites 08 and 09.

The resistivity model suggests a limit (L1) at a depth of 1.7–1.8 km at the western end of the profile, below site 1 and site 2. This limit is interpreted as the base of the Nachukui Formation. Towards the East, this limit is shallower (at ~1.2–1.4 km depth) under sites 4 and5. The bottom of the upper low density layer is deeper than the limit L1 in the resistivity model (Fig 12ab) suggesting that this limit is probably deeper than indicated by the resistivity.

Under site 5 (Fig. 12a), a resistive heterogeneity, visible between ~100-150 m depth

down to 600-700 m depth within the Nachukui/Kibish Formations, has no signature in term of density contrast, which suggests that it is an artefact.

A possible interface (L2), supposed to be boundary between the “Turkana Volcanics” and the Lapur Sandstone and/or the Precambrian basement (Fig. 2c) is suggested in Figure 12a while Figure 12b (the density model) suggests that this limit could be in fact L1. The resistive body beneath sites 6-9 has a density contrast slightly positive which would agree with either highly fractured volcanics or the Lapur sandstone or both. Eastward, this limit is not clearly identified in the resistivity model. Precambrian basement might form the base of the resistivity model, especially under sites 05 to 09.

Our interpretation suggests that the thickness of the Plio-Pleistocene/Holocene sediments in southern profile is larger than in profile P2. The depth of this limit between the sediments and the “Turkana Volcanics” decreases eastwards through a system of normal faults including the main MRL Border Fault and the F2S and F3S Faults. The chrono-stratigraphy visible at the MRL Border Fault suggests that volcanics overlying the Lapur Sandstone should be present but not distinct in our results (Fig. 12).

The significant thickness (2 km or more) of the Plio-Pleistocene/Holocene sediments, as suggested by the seismic interpretation, is clearly revealed in both resistivity and density models immediately to the east of the F3S Fault, and can be extended offshore Lake Turkana as observed in northern profile (Fig. 10). This interpretation is close to that proposed by Tiercelin et al. (2012a; Fig. 15, p. 62) achieved on the TVK-10 seismic line, which suggests the presence in the MRL hanging wall of an important pile of sediments, probably underlain by the ‘‘Turkana Volcanics’’, and a sediment package including the Lapur Sandstone.

8. Subsurface structure of the Kachoda Valley

The resistivity and the density sections for the Kachoda Valley (Figs. 1b and d) are presented in Figure 13. The models are more complex and on average more resistive and dense than for profiles P1-P3. In Figure 13a, we identify the possible signature of several faults. On the West side of the profile, we defined F1W between sites 18 and 19; and F2W , located under site 20 and which may reach a depth of >5 km. In the center of the profile, F3W between sites 21 and 22 is uncertain. To the East, F4W is beneath site 23 and F5W beneath site 24, also reaching a depth >5 km.

To the West, between sites 18 and 19 from the surface to ~1.5 km we observe an upper conductor over a resistive bedrock. We interpret this limit (named L1') as the base of the surface sediments probably intermingled with dikes and sills (because of the positive density contrast) overlying the "Turkana Volcanics". The sediment layer thins eastward and reaches 1 km depth under site 20. W. The resistivity values from surface down to (L1') limit do not exceed 10 Ω.m (Fig. 13). Below the (L1') limit, the resistivity values range between 20 and 70-80 Ω.m. We hypothesize that the limit (L2) marking the transition between the "Turkana Volcanics" and the Lapur Sandstone and/or the Precambrian basement, is identified under limit (L1'), This limit (L2) seems identifiable in both resistivity and density models between the Lokitaung Gorge and the eastern end of the Kachoda Basin (beneath sites 21 and 22, Fig 13a).

The stratigraphic contact between the Lapur Sandstone and the "Turkana Volcanics" outcrop on the right bank of the Lokitaung Gorge immediately west of station 24 at lat. 04° 16' 04" N and long. 35° 47' 34" E (Figs. 2c, 13c). Thus station 24 is located directly on the Lapur Sandstone while station 23 is located on the overlying "Turkana Volcanics". From the resistivity model (Fig. 13a), the resistivity values beneath these sites are greater than 50 Ω.m while the density contrast is slightly negative. This observation outlines the difficulty

in distinguishing the Precambrian basement from the Lapur Sandstone, as both formations are characterized by high resistivity values.

This profile is very heterogeneous. The structures seem controlled by the faults identified in Figure 13a. In particular, the 1.5-1.6 km thick sediment infill of the Kachoda basin can be compared to a part of the Plio-Pleistocene/Holocene sediment infill existing in the nearby Turkana Basin.

9. Subsurface geological models

From the density and resistivity models obtained in this study as well as the available information as outcrops and known chrono-stratigraphical data, we propose a series of conceptual geological models along the three profiles of the Turkana Basin and the Kachoda Basin (Figs. 10d-13d and 14).

Figure 14

The proposed geological model for the northern profile is illustrated on Fig. 10d. As identified by the density and the resistivity models, and by geological data collected at the outcrop level in the Lapur Range, the main MRL Border Fault is clearly located and its dip is confirmed. Two other faults, F0N and F3N, are suggested in the western and eastern parts of the profile, as well two other faults, F1N and F2N, located in the central part of the profile. These faults have no surface expression and thus may be considered as inactive today. The main MRL Border Fault bounds the Plio-Pleistocene and Holocene sediment infill of the Turkana Basin to the west, i.e. the Nachukui and Kibish Formations. This sediment infill (corresponding to the lowest resistivity and density contrasts) does not

exceed a total thickness of ~1.5 km at the western end of the profile and decreases in thickness to about 1 km toward the east, at 2.5 km to the west of the Lake Turkana shoreline, on the western side of the F3N Fault. To the east of the F3N Fault, towards Lake Turkana, the thickness of these sediments reaches up to 3-5 km. Below these Plio-Pleistocene/Holocene (and possibly older?) sediments should lie the "Turkana Volcanics" unit. However, the density model does not show values in agreement with volcanics unless the later are strongly fractured or very thin. According to field observations (Tiercelin et al., 2012a), the "Turkana Volcanics" should be underlain in the area of the Lapur Peak by a maximum of 0.100-120 m of Lapur Sandstone (Figs. 2a and 3a). The thickness of the Lapur Sandstone may vary accordingly to the topography of the top of the basement. The basement should lie below the Lapur Sandstone and from the MRL Border Fault. The low density observed in the whole section excepted at the westernmost side suggests however that the material below Plio-Pleistocene and Holocene sediment could be sediments rather than Turkana volcanics. The thickness of the sediments is similar to the thicknesses observed on the PROBE seismic lines as well as on the Eliye Springs-1 well. This significant sediment thickness could be explained as the result of a major subsidence associated to a high sedimentation rate along the F3N Fault, which thus could be considered as the main border fault of the Turkana Basin activated during at least the Pliocene and Pleistocene/Holocene periods, compared with the main MRL Border Fault and the other secondary faults. Alternatively, the northern profile stands near the acknowledged interfering rifts between the Miocene to actual rift and older rift system running from the Anza into the Muglad-Melut systems (Fig.1). Accumulation of Pliocene and Pleistocene/Holocene sediments over cretaceous-holocene units could explain both the resistivity and density distribution beneath sites 13-17 (Figure 10ab). This interpretation is supported by recent gravity and magnetic surveys carried out over the Turkana Depression

(Hutshinson et al., 2010).

On the eastern part of the profile, close to the Lake Turkana shoreline, the resistivity and density models do not show clear vertical contrast that could be used to distinguish sediments from the volcanic rocks, or any other interface below, to the exception of the limit (L0), which is characterized by a clear contrast in the density model, with nevertheless a poor contrast in terms of resistivity. This limit could correspond to a wide saline water intrusion (e.g. Johnson et al., 1987), which is limited to the west by the F3N Fault. In this part of the profile, more than 3 km of Plio-Pleistocene/Holocene (or older?) sediments identified.

At the bottom of the models we identified two structures (A and B) in Figs. 10a-b at the depth of 3-4 km and 2-3 km, respectively. These structures are limited in space, conductive and low density. Partial fusion of the basement is unlikely because it is shallow and the density is small (negative contrast of 120 kg m^{-3} for B and 180 kg m^{-3} for A). If the hypothesis of sediment accumulation through the conjunction of the EAR and Anza rift in the Turkana depression is correct, these structures could be small-scale depocenters. Their signature is similar to gravity and resistivity structures for depocenters observed in other regions but deeper (e.g. Hautot et al., 2007).

The proposed geological model for the central profile (P2 and Kachoda) is presented in Figs. 11d, 13d and 14. East of the escarpment toward Lake Turkana, The MRL Border Fault seems to have a clear signature in both the resistivity and density models. A major west-dipping structure (between sites 11 and 25) can be observed also in both models East of the MRL Border Fault. The resistivity and density values obtained for this structure are similar to those for the MRL fault region. The resistive body (beneath sites 10 and 11) outcrops is from the “Turkana Volcanics” unit (Tiercelin et al. 2012a). Thus, this structure could be interpreted as a large volcanic intrusion, possibly a wide volcanic dyke or a large

sill, both structures being well represented in the area of the Lapur Range (Fig. 3f) (Tiercelin et al., 2012a) (Fig. 11d). East F2C (Figure 11a), the resistivity and density models support the stratigraphic sequence observed on the escarpment (Figure 2b) unlike for the northern profile. We observe a variation in thickness of the Plio-Pleistocene/Holocene sediments and the “Turkana Volcanics” from ~0.5-0.6 km to ~0.8 k for the Plio-Pleistocene/Holocene sediments then remains relatively constant eastward of F3C. The thickness of the “Turkana Volcanics” unit varies from ~0.5-1.5 km. A maximum thickness of ~500 m of Lapur Sandstone could be present downward from the (L2), with the same dip as the “Turkana Volcanics” (Fig. 11d), but cannot be clearly imaged in this study.

The Kachoda Basin is well identified at the western end of the central profile (Figs. 13d and 14). The upper part of the basin infill is characterized by sediments with a maximum thickness of ~1.5-1.6 km (possibly the same sediments as those of Turkana Basin?). Below this pile of sediments is a package of “Turkana Volcanics”, the thickness of which remains uncertain because the (L2) limit is not precisely defined in this part of the model. However, a thickness value of >2 km is expected under the sites 21 and 22. Under the “Turkana Volcanics”, a maximum thickness of ~0.5 km can be expected for the Lapur Sandstone under site 24 and immediately to the west, as it is in the area of the Lokitaung Gorge (Thuo, 2009; Tiercelin et al., 2012a) (Fig. 2b). If the Lapur Sandstone exists in the subsurface of the Kachoda Basin, it will show lateral variations of thickness according to the changing morphology (of topographic or tectonic origin) of the top of the basement. Between the Turkana and Kachoda Basins, no obvious geological interpretation can really be provided. A strong thinning of the Lapur Sandstone can be envisaged below the Kachoda Basin. In the nearby Gatome half-graben (Fig. 1a), the presence of Cretaceous?-Paleogene sediments is suggested by seismic reflection data but cannot be related directly to the Lapur Sandstone

(Wescott et al., 1999; Tiercelin et al., 2012a).

The proposed geological model of the southern profile (Fig 12d and 14) presents a stratigraphy similar to the central profile with a thicker Plio-Pleistocene/Holocene sediment cover (2-2.5 km). (Fig. 12d) The thickness value of the “Turkana Volcanics” is difficult to assess because neither the resistivity or the density model show clear transitions between the volcanics, a possible Lapur sandstone layer and the

The conceptual geological model presented in Fig. 14, mainly for the southern profile, is generally in agreement with the recent re-interpretation of the TVK-10 seismic line (Tiercelin et al., 2012; Fig. 15) in terms of geometries, depths and thicknesses of the Plio-Pleistocene/Holocene sediments, the “Turkana Volcanics”, Lapur Sandstone and Precambrian basement.

The rapid structural changes in the resistivity and density models from the central profile to the northern profile is supported by the recent gravity and magnetic surveys carried out over the whole Turkana depression region (Hutchinson et al., 2010). The density model suggests that the imaged substratum is filled by sediments down to at least 5 km. The resistivity model completes the picture with a clear limit between highly conductive Plio-Pleistocene/Holocene sediments and more resistive, probably older (cretaceaous-holocene?) sediments maybe to be related to the Gatome Cretaceous?-Paleogene sediments.

10. Hydrocarbon implications

Following our study in the northwest part of the Turkana Basin, the highest potential area in terms of oil exploration can be found in the northern profile, along the shoreline of Lake Turkana, where the presence of ~3-5 km of sediments of Plio-Pleistocene age topping probably older sediment is imaged. This thick sedimentary pile may contain alternating sequences of potential source rocks and reservoirs, as it is the case in the oil-rich Lake

Albert Basin in the western branch of the EARS. Also, in the nearby South Omo Block in Southern Ethiopia, the Sabisa-1 well (~10 km immediately north of Turkana Lake) recently drilled by Tullow Oil and Africa Oil Corporation reached a total depth of 1810 metres and encountered “reservoir quality sands, oil shows and heavy gas shows indicating an oil prone source rock and a thick shale section”. Below the recent ~2km sediment accumulation in the North Turkana Basin the locally thick pile of “Turkana Volcanics” if present seems very thin but still could act as a seal for the underlying Lapur Sandstone, which demonstrates good reservoir qualities based on results of porosity measurements (3-25%) (Thuo, 2009). The interfering rifts of the Turkana depression (Hutshinson et al. 2010) may be at the origin of a thick pile of possibly creataceous-holocene sediments. Thus, considering the regional oil potential, e.g. the nearby South Sudan oil fields, and the promising South Lokichar Basin, the North Turkana area appears as a region of major interest for oil and gas exploration in the Eastern Branch of the EARS.

More effort must be devoted combining seismic and non-seismic techniques to get more information about the existence in the Turkana region of good quality reservoirs and trapping mechanisms as well the identification of mature source rocks necessary to support a working petroleum system.

11. Conclusions

The major results of this study in terms of subsurface structure and stratigraphy of the North Turkana Basin can be summarized as follows:

1) The resistivity and density models provided by MT and gravity joint inversion have clearly confirmed the half-graben geometry of the northwest end of the Turkana Basin, with the identification, in addition to the main MRL Border Fault, of three main synthetic faults (F1, F2 and F3) which today have no surface expression. Taking into account the thick

sediment accumulation (>3 km) in their respective hanging walls, the F3 Fault and the MRL Border Fault can be considered as being the main border faults of the North Turkana Basin at least for the Mio-Pliocene period for the MRL Fault, and for the Plio-Pleistocene period for the F3 Fault. This may suggest a migration of rift tectonics from west to east since Middle Miocene (initiation of the MRL Border Fault).

2) Characterization of a newly defined half-graben basin located to the immediate west of the Turkana Basin, named the Kachoda Basin, in terms of structure and subsurface stratigraphy. The main conclusion for the Kachoda half-graben is the presence within the basin of a 1.5 km thick pile of sediments that may represent a stratigraphic equivalent of the Plio-Pleistocene/Holocene Nachukui and Kibish Formations, both deposited in the nearby Turkana Basin. The Kachoda sedimentary infill may relate to a suite of major transgressive phases of Lake Turkana within the Kachoda Basin during the Plio-Pleistocene or even older periods. Underlying these sediments, a maximum of 1.5 km of volcanic rocks belonging to the "Turkana Volcanics" has been identified.

3) Important lateral variations in the thickness of the "Turkana Volcanics" from west to east and from south to north along the three profiles are also clearly evidenced.

4) The stratigraphic contact (L2) between the "Turkana Volcanics" and the underlying Lapur Sandstone and/or Precambrian basement is partly identified in the different profiles. The presence of the Lapur Sandstone in the Turkana Basin, and in the Kachoda Basin, nevertheless, remains unresolved because the difficulty to separate the geophysical response of the Precambrian basement and Lapur Sandstone.

5) Strong lateral variations in thickness of the Plio-Pleistocene and Holocene sediment and possibly older sediments to the North infill of the Turkana Basin (the Nachukui/Kibish Formations), from west to east and from south to north. From 1.5 km at the west end of the northern profile to >3 km at its east end, in the hanging wall of the F3C Fault, almost

offshore Lake Turkana

6) Additionally, the proposed models also help to resolve ambiguities met in previous interpretations. In particular, the reflection seismic method previously used in the Lotikipi, Gatome, Turkana and Lokichar Basins has demonstrated difficulty in determining the thickness of volcanic rocks below a thick sediment pile, as well as imaging the stratigraphy and structures below thick piles of volcanic rocks (the well-known sub-basalt imaging problem, e.g. Ziolkowski et al., 2003) (e. g., Wescott et al., 1999; Tiercelin et al., 2012a).

Acknowledgements

This work is part of Yassine Abdelfettah's PhD thesis, funded by the Ministry of Research in France. The University of Neuchâtel-Switzerland, Karlsruhe Institute for Technology (KIT-INE) – Germany and the IPGS/EOST – University of Strasbourg – France financed partly this work. The field experiment was mainly funded by the Cooperation and Cultural Affairs Service of the French Embassy in Kenya. The authors are particularly grateful to Franck Humbert and Serge Snrech, Cooperation and Cultural Action Counsellors at the French Embassy in Kenya, Nairobi, for their continuous encouragements. Logistical support such as geophysical equipment and 4-wheel drive vehicles was provided by the Kenya Electricity Generating Company (KenGen) and the National Oil Corporation of Kenya (NOCK). Special thanks are due to Silas M. Simiyu, KenGen Geothermal Development Manager, and to Mrs Mary M'Mukindia, NOCK Managing Director. Field contribution of KenGen and NOCK personnel is gratefully acknowledged. Permission to conduct field geological research in the West Turkana Basin was provided by the Office of the President and the Ministry of Education, Science and Technology of the Republic of Kenya (Research Permits to JJT, Nos. OP/13/001/23C 290 and MOEST 13/001/23C 290). Dr. Niels Giroud and Dr. Mathieu Schuster are thanked for

their help to improve the clarity of the manuscript. Dr. Gallardo Luis A. is thanked for his reading and correcting the joint inversion methodology part in previous version, which help us to improve the clarity of the developed joint inversion approach.

REFERENCES

Abdelfettah, Y., 2009. Inversion conjointe des données magnétotelluriques et gravimétriques : Application à l'imagerie géophysique crustale et mantellique. Thèse de l'Université de Bretagne Occidentale, Brest, France, 171 p. <http://tel.archives-ouvertes.fr/docs/00/42:44/13/PDF/These_Yassine_a_imprimer.pdf>.

Africa Oil Corporation, 2011. Hunting for Elephants in East Africa's Rift Basins. Accessed 24th February 2014, http://www.africaoilcorp.com/i/pdf/AOI-Hunting-Elephants-October-2011.pdf

Africa Oil Corporation, 2014. String of pearls-Well summary. Accessed 15th August 2014, http://www.africaoilcorp.com/i/pdf/AOI-well-summary.pdf

Bellieni, G., Justin-Visentin, E., Zanettin, B., Piccirillo, E.M., Radicati di Brozolo, F., Rita, F., 1981. Oligocene transitional-tholeiitic magmatism in northern Turkana (Kenya). Comparison with the coeval Ethiopian volcanism. Bulletin of Volcanology 44, 411-427.

Chave, A.D., Thomson, D.J., 2004. Bounded influence estimation of magnetotelluric response functions Bounded influence magnetotelluric response function estimation. Geophysical Journal International, 157, 988-1006.

Counil, J., Lemouel, J., Menvielle, M., 1986. Associate and conjugate directions concepts in magnetotellurics. Annales Geophysicae series B-terrestrial and Planetary Physics 4, 115-130.

788 Dunkelman, T.J., Karson, J.A., Rosendahl, B.R., 1988. Structural style of the Turkana Rift,
789 Kenya. Geology 16, 258-261.

790 Dunkelman, T.J., Rosendahl, B.R., Karson, J.A., 1989. Structure and stratigraphy of the
791 Turkana rift from seismic reflection data. Journal of African Earth Sciences 8, 489–510.
792 http://dx.doi.org/10.1016/S0899-5362(89)80041-7.

793 Dunkley, P. N., Smith, M., Allen, D. J., Darling, W. G., 1993. The geothermal activity and
794 geology of northern sector of the Kenya rift valley. British Geological Surveys,
795 Research Report SC/93/1, 118-133.

796 East African Topographic Map, 1972. 1:250,000, Series Y503, Sheet NB-36-16, Edition 2-
797 SK, Lokitaung, published by Survey of Kenya.

798 Ebinger, C.J., Ibrahim, A., 1995. Multiple episodes of rifting in Central and East Africa: a re-
799 evaluation of gravity data. Geologische Rundschau 83, 689-702.

800 Ebinger, C. J., Yemane, T., Harding, D. J., Tesfaye, S., Kelley, S., & Rex, D. C., 2000. Rift
801 deflection, migration, and propagation: Linkage of the Ethiopian and eastern rifts,
802 Africa. Bulletin of the Geological Society of America, 112, 163–176.

803 Feibel, C.S., Brown, F.H., McDougall, I., 1989. Stratigraphic context of fossil hominids from
804 the Omo Group deposits, northern Turkana Basin, Kenya and Ethiopia. American
805 Journal of Physical Anthropology 78, 595-622.

806 Furman, T., Bryce, J. G., Karson, J., Iotti, A., 2004. East African Rift System (EARS) plume
807 structure: insights from Quaternary mafic lavas of Turkana, Kenya. Journal of Petrology
808 45, 1069–1088.

809 Groom, R.W., Bailey, R.C., 1989. Decomposition of magnetotelluric impedance tensors in
810 the presence of local three-dimensional galvanic distortion, J. Geophys. Res., 94, 1913-
811 1925.

Goubau, W.M., Gamble, T.D., Clarke, J., 1978. Magnetotelluric data analysis: removal of bias. Geophysics, 43(6), 1157-1166. doi: 10.1190/1.1440885.

Hautot, S., Single, R. T., Watson, J., Harrop, N., Jerram, D. A., Tarits, P., Whaler, K., Dawes, G., 2007 - 3-D magnetotelluric inversion and model validation with gravity data for the investigation of flood basalts and associated volcanic rifted margins, Geophysical Journal International, 170, 1418-1430.

Hutchinson, I., Lawrence, S., Beach, A., 2010. Interfering Cretaceous and Tertiary Rift Systems of the Turkana Depression (Sudan-Ethiopia-Kenya), Houston Geological Society Bulletin, Volume 52, No. 8, April 19, 2010. 32-37.

Johnson, T.C., Halfman, J.D., Rosendahl, B.R, Lister G.S., 1987. Climatic and tectonic effects on sedimentation in a rift-valley lake: Evidence from high-resolution seismic profiles, Lake Turkana, Kenya. Geological Society of America Bulletin, 98, 439-447.

McDougall, I., Brown, F.H., Fleagle, J.G., 2005. Stratigraphic placement and age of modern humans from Kibish, Ethiopia. Nature 433, 733-736.

McNeice, G.W., Jones, A.G., 2001. Multi-site, multi-frequency tensor decomposition of magnetotelluric data. Geophysics, 66, 158-173.

Morley, C.K., 1999. Influence of pre-existing fabrics on rift structure. In: Morley C.K. (Ed.), Geoscience of Rift Systems - Evolution of East Africa. American Association of Petroleum Geologists Studies in Geology 44, pp. 151-160.

Morley, C.K., Wescott, W.A., Stone, D.M., Harper, R.M., Wigger, S.T., Karanja, F.M., 1992. Tectonic evolution of the northern Kenyan rift. Journal of the Geological Society 149, 333-348.

Parker, R.L., 2011. New analytic solutions for the 2-D TE mode MT problem; Geophysical Journal International 186, 980-986, doi: 10.1111/j.1365-246X.2011.05091.x

Simpson, F., and Bahr, K., 2005. Practical Magnetotellurics. Cambridge: Cambridge University Press, p. 270.

Talbot, M.R., Morley, C.K., Tiercelin, J.-J., Le Hérissé, A., Potdevin, J.-L., Le Gall, B., 2004. Hydrocarbon potential of the Meso-Cenozoic Turkana depression, northern Kenya. II. Source rocks: quality, maturation, depositional environments and structural control. Marine Petroleum Geology 21, 63-78.

Tiercelin, J.-J., Potdevin, J.-L., Morley, C.K., Talbot, M.R., Bellon, H., Rio, A., Le Gall, B., Vétel, W., 2004. Hydrocarbon potential of the Meso-Cenozoic Turkana depression, northern Kenya. I. Reservoirs: depositional environments, diagenetic characteristics, and source rock-reservoir relationships. Marine Petroleum Geology 21, 41-62.

Tiercelin, J.-J., Potdevin, J.-L., Thuo, P. K., Abdelfettah, Y., Schuster, M., Bourquin, S., Bellon, H., Clément, J.-P., Guillou, H., Nalpas, T., Ruffet, G., 2012a. Stratigraphy, sedimentology and diagenetic evolution of the Lapur Sandstone in northern Kenya: Implications for oil exploration of the Meso-Cenozoic Turkana depression. Journal of African Earth Sciences 71-72, 1-37.

Tiercelin, J.-J., Thuo, P., Potdevin, J., Nalpas, T., 2012b. Hydrocarbon Prospectivity in Mesozoic and Early-Middle Cenozoic Rift Basins of Central and Northern Kenya, Eastern Africa. In: Gao, D. (Ed.), Tectonics and Sedimentation: Implications for Petroleum Systems, American Association of Petroleum Geologists Memoir 100, pp. 1-29.

Thuo P., 2009. Stratigraphic, Petrographic and Diagenetic Evaluation of Cretaceous/Paleogene

Potential Reservoir Sandstones of Western Turkana, Kenya. Implications on the Petroleum Potential of Northwestern Kenya. Thèse de l'Université de Bretagne Occidentale, Brest, France, 139 p.

Walsh, J., Dodson, R.G., 1969. Geology of Northern Turkana. Report Geological Survey of Kenya 82, 42 p.

Wescott, W.A., Wigger, S.T., Stone, D.M., Morley, C.K., 1999. Geology and geophysics of the Lotikipi plain. In: Morley C.K. (Ed.), Geoscience of Rift Systems - Evolution of East Africa. American Association of Petroleum Geologists Studies in Geology 44, pp. 55-65.

Zanettin, B., Justin Visentin, E., Bellieni, G., Piccirillo, E.M., Rita, F., 1983. Le volcanisme du Bassin du Nord-Turkana (Kenya) : Age, succession et évolution structurale. In: Popoff, M., Tiercelin, J.-J., (Eds.), Rifts et Fossés anciens. Bulletin des Centres de Recherches Exploration-Production Elf-Aquitaine 7, 249-255.

Ziolkowski, A., Hanssen, P., Gatliff, R., Jakubowicz, H., Dobson, A., Hampson, G., Li, X-Y., Liu, E., 2003. Use of low frequencies for sub-basalt imaging, Geophysical Prospecting 51, pp. 169-182.

List of figures

Fig. 1. (a) Schematic map showing the distribution of Cretaceous–Paleogene to Neogene rift basins in southern Sudan, southern Ethiopia and northern, central and eastern Kenya. Intense oil exploration is presently conducted in all these regions. In the Northern Kenya Rift, several N-S-trending sedimentary basins of Cretaceous?-Paleogene to Plio-Pleistocene age - the Lotikipi, Gatome, Lokichar (North and South),

North Kerio and Turkana Basins - have been identified using gravity and seismic reflection methods. In the Lokichar Basin, in addition to the Loperot-1 well (drilled in 1992), and the Ngamia-1 well (drilled in 2010) (indicated by a black dot and a black star, respectively), several other highly promising exploration wells have been drilled recently in the South Lokichar Basin (modified from Ebinger and Ibrahim, 1995; Morley et al., 1999; Wescott et al., 1999; Tiercelin et al., 2004; Africa Oil Corporation, 2011, 2014). The white box/black arrow indicates the study area. (b) Block-diagram of the study area, showing the MT and gravity measurement sites along the three profiles P1 (southern), P2 (central) and P3 (northern). SRTM30 (Shuttle Radar Topography Mission of 30 m resolution) is used as a topography model and the vertical exaggeration is about 9 times (900 %). The numbers refer to the MT stations. (c) Regional map of the Lake Turkana Basin, showing outcrop areas of the Plio-Pleistocene ‘‘Omo Group” deposits, that include the Nachukui Formation in the northwest part of the Turkana Basin. The sediments of the Kibish Formation type-section outcrop further north, on the right bank of the Omo River. The 2.9-km deep Eliye Springs-1 well is indicated east of the town of Lodwar by a small rig. Older sedimentary deposits (Paleogene to Pliocene) outcrop at the southwest end of the Turkana Basin (redrawn from Feibel et al., 1989; Morley et al., 1999; McDougall et al., 2005). (d) Topographic map (scale 1:250,000) of the northwest part of the Turkana Basin, showing the Kachoda Valley, the Lapur Range and the Murua Rith Hills that bound the northwestern half of the Turkana Basin (i.e. the Murua Rith-Lapur Rift Border Fault). Geological/geophysical cross-sections, seismic lines and geographic sites cited in the text are indicated (from East African Topographic Map, 1972).

Fig. 2. Interpretative geological cross-sections perpendicular to the western, N-S-

trending faulted side of the North Turkana Basin, based on the geological map established by Walsh and Dodson (1969), seismic lines interpretations (Wescott et al., 1999; Tiercelin et al., 2012a) and fieldwork. The three geophysical profiles are superimposed on these geological cross-sections, respectively: the southern profile P1 (which is also superimposed to the trace of the TVK-10 seismic line acquired by the Amoco Company), the central profile P2, and the northern profile P3. For the southern profile, the interpretation of the TVK-10 seismic line in the hanging wall of the MRL Border Fault is deduced from Wescott et al. (1999). On the 3 geological cross-sections, the continuous grey line represents the geophysical profiles, and the x-axis represents the distance (km) from the western shore of Lake Turkana. The dashed boxes delineate the study areas where the conceptual geological models (see Fig. 12) will be considered.

Fig. 3. (a) General view from the east (Todenyang Plain) of the 1600 m high Lapur Range, showing the Lapur Sandstone (LS) overlying the Precambrian basement (marked by the yellow bold dashed line) between 04°20’ and 04°35’ N. In the region of the Lapur Peak (Figs. 1d and 2a), the Lapur Sandstone is about 100-120 m thick and forms the upper part of the Lapur Range, which corresponds to the Murua Rith-Lapur Border Fault escarpment that bounds the Turkana rift basin to the northwest. On the photo, the trace of the MRL Border Fault is marked by a yellow dashed line. The two peaks that dominate the LS cliff on the far horizon correspond to outcrops of lavas belonging to the « Turkana Volcanics » (TV), overlying the Lapur Sandstone. See Fig. 1b and d for the location of the P3 profile across the Todenyang Plain. (b) View of the middle and upper parts of the Lapur Sandstone to the immediate north of the Lokitaung Gorge, at about 15 km south of Lapur Peak (see Fig. 2a and b). In this area,

the Lapur Sandstone is 500 m thick and overlies the Precambrian basement that outcrops a few kilometres to the north (see (a), yellow bold dashed line). (c) Detailed view of the stratigraphic contact (indicated by the yellow dashed line) between upper beds of the Lapur Sandstone and the lowermost flows of the ‘‘Turkana Volcanics’’, visible on the right bank of the Lokitaung Gorge at 04°16’ 04’’ N; 35°47’ 34’’ E (LG; see Figs. 1d and 2b for location). (d) Fluvio-deltaic sediments belonging to the Plio-Pleistocene Nachukui Formation that forms a large part of the infill of the North Turkana Basin. (e), (f) Large cooling structures such as columnar jointing (e) and tores (f) are well developed within the basaltic flows of the ‘‘Turkana Volcanics’’, and may explain the observed low average resistivity values. (g) Wide volcanic dykes and thick sills are abundant in the area of the P2 and P3 profiles (Lokitaung Gorge, Kerral area and north of Lapur Peak) and in the Keniroliom area south of the P1 profile (Fig. 1d). The (f) picture presents a view of a 10-m wide N60°-trending tephritic dyke crosscutting the upper beds of the Lapur Sandstone in the Kerral area (see location Fig. 1d). This dyke (marked by the black boulders on the photo) is dated 27.03 ± 0.57 Ma (from Tiercelin et al., 2012a). Larger dykes (up to 70 m) are known in the northern part of the Turkana Basin as well as in Southern Ethiopia (Ebinger et al., 2000).

Fig. 4. Re-interpretation of the TVK-10 seismic line (from Tiercelin et al., 2012a), presenting the possible presence in the hanging wall of the MRL Border Fault, below the ‘‘Turkana Volcanics’’ (marked at top by a bold dashed line and at base by a dotted line), of a 300-m thick sedimentary package that can be interpreted as the Lapur Sandstone (marked at base by a dashed/dotted line). The ‘‘Turkana Volcanics’’ are in turn overlain by hundreds of metres of fluvio-lacustrine sediments of Plio-Pleistocene age forming the uppermost part of the infill of the Turkana Basin (i.e. the Nachukui

Formation).

Fig. 5. MT and gravity field experiments showing the used materials to record datas. a) and b) gravity data acquisition using Lacoste-Romberg gravimeter. c) Phoenix datalogger used to record MT time series. d) and e) showed coil used to record magnetic field and probe used to record electrical field, respectively.

Fig. 6. Resistivity and phase fits recovered from magnetotelluric measurements. Symbols stand for the observed data and continuous lines for model. (a) Apparent resistivity and (b) phase fit for MT sites for the three profiles responses, where a good fit was obtained between observed and computed apparent resistivities and phases, especially in the small periods where the information for shallow subsurface concerning this study could be obtained. Red and blue colours represent the TM and TE modes, respectively. The error bars are the 68 % confidence interval.

Fig. 7. Maximum electrical field direction (MED) at each site at the period T=0.5 s (yellow) and 50 s (red). The width of the pie wedge is two standard deviations. The length of the pie wedge is a function of the ratio between the maximum and minimum impedance tensor. Larger values indicate well-defined maximum electrical field direction. SRTM 30 m (Shuttle Radar Topography Mission, 30 m of resolution) is used in the background.

Fig. 8. Gravity data fit. Symbols stand for the observed data and continuous lines for model responses. Free air anomalies obtained for the northern, central and southern profiles.

Fig. 9. Model parameterisation and geometrical constraint defined by the GCF. The resistivity parameters are grouped in a limited number of domains (here 3 domains). The horizontal and vertical lines represent the 2-D grid. The parameters mr_{ij} and md_k are the resistivity of the ijth block and the density value of kth domain, respectively.

Fig. 10. (a) Resistivity model, and (b) density model obtained by MT and gravity joint inversion for the northern profile (P3) (Fig. 1b). The dashed lines represent the major resistivity and density contrasts or uncertain fault extensions. (c) the major resistivity and density visible in the obtained results as well as major faults. (d) The final conceptual geological model proposed for this profile.

Fig. 11. (a) Resistivity model and (b) density model obtained by MT and gravity joint inversion for the segment of the central profile located in the Turkana Basin (eastern part of Profile 2 on Fig. 1b). The dashed lines represent the major resistivity and density contrasts or uncertain fault extensions (c). This held to the final conceptual geological model showed in (d).

Fig. 12. (a) Resistivity model, and (b) density model obtained by MT and gravity joint inversion for the southern profile (P1) (Fig. 1b). The dashed lines represent the major resistivity and density contrasts or uncertain fault extensions. (c) the major resistivity and density visible in the obtained results as well as major faults. (d) The final conceptual geological model proposed for this profile.

Fig. 13. (a) Resistivity model, and (b) density model obtained by MT and gravity joint inversion for the central profile (P2) in the Kachoda Basin (western part of the profile;

Fig. 1b). The dashed lines represent the major resistivity and density contrasts or uncertain fault extension. (c) the major resistivity and density visible in the obtained results as well as major faults. (d) The final conceptual geological model proposed for this profile.

Fig. 14. Conceptual geological models proposed for the central profile including both Turkana and Kachoda basins. These conceptual models are derived using resistivity and density models obtained in this study, as well as the available geological knowledge provided mainly from the fieldwork.

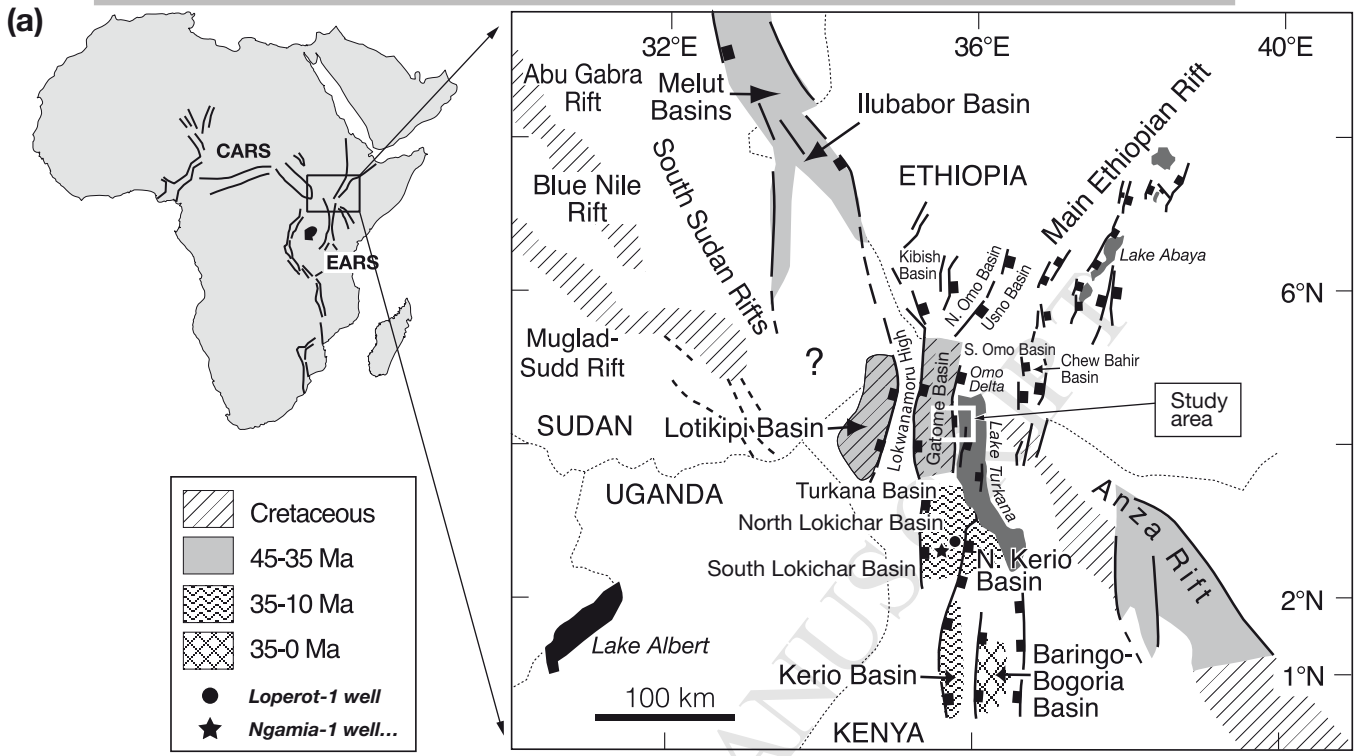

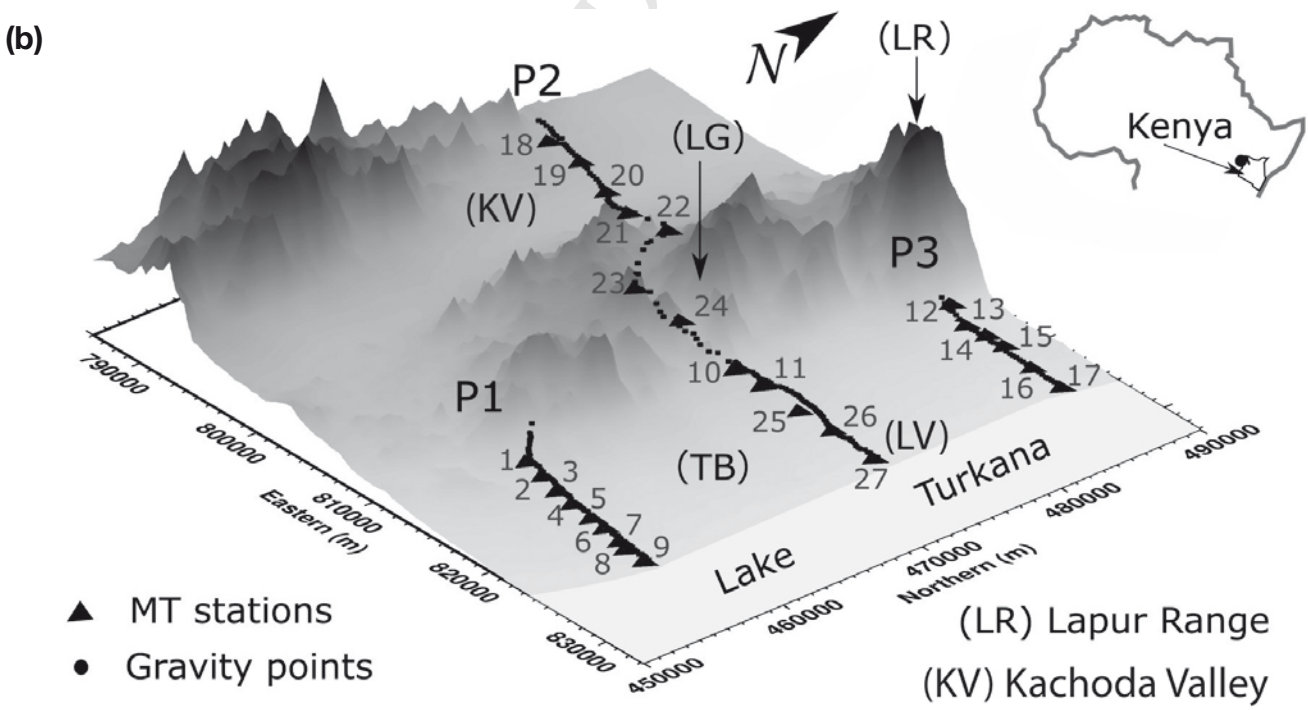

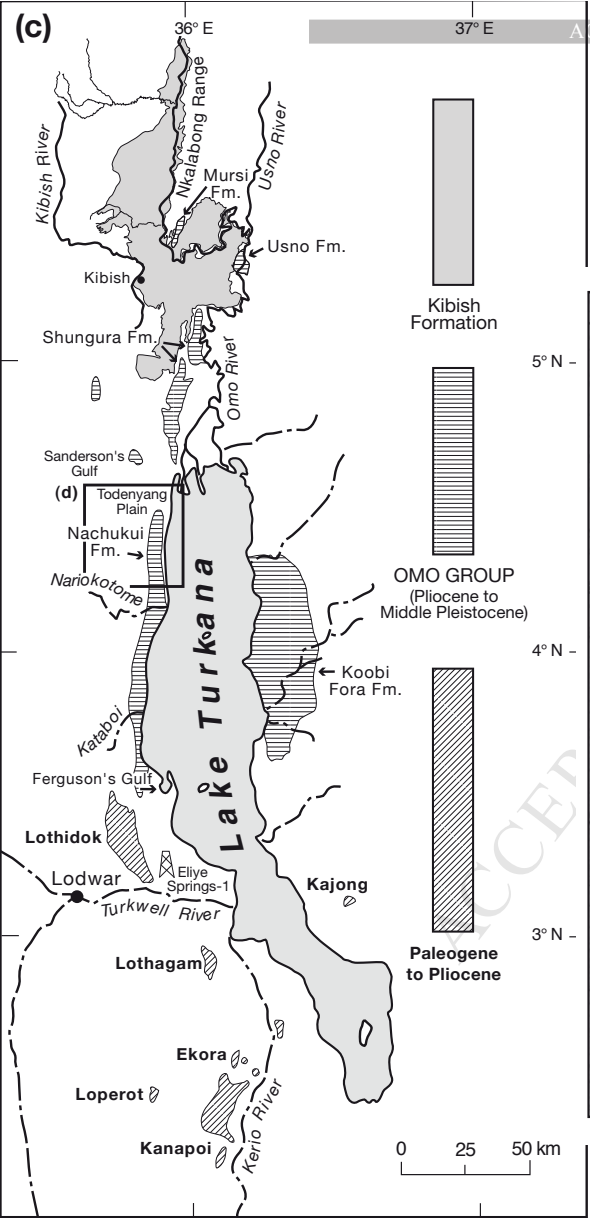

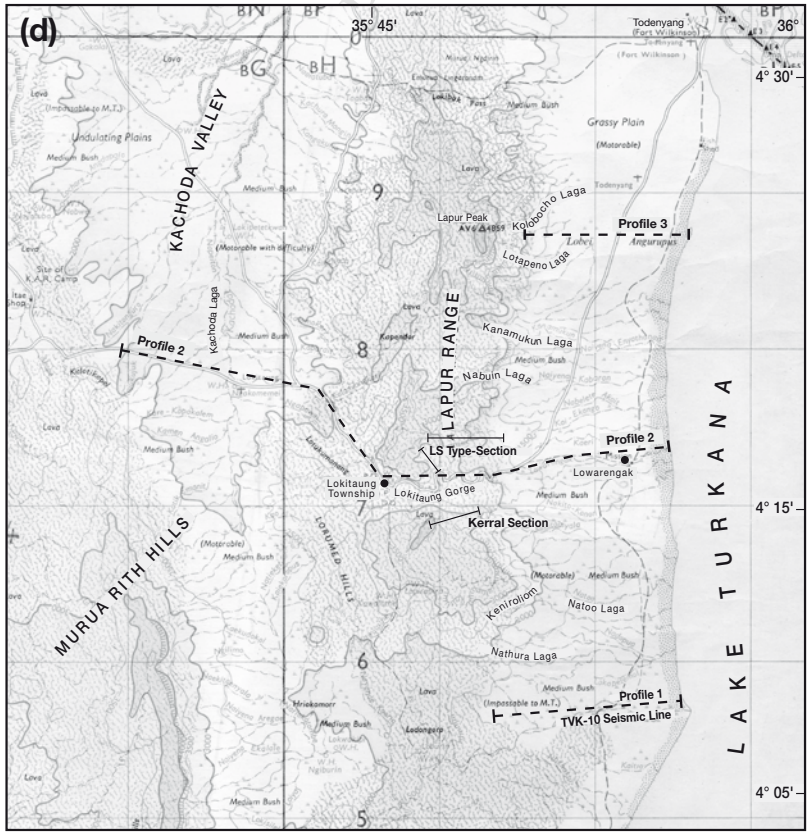

(a) Northern geological profile

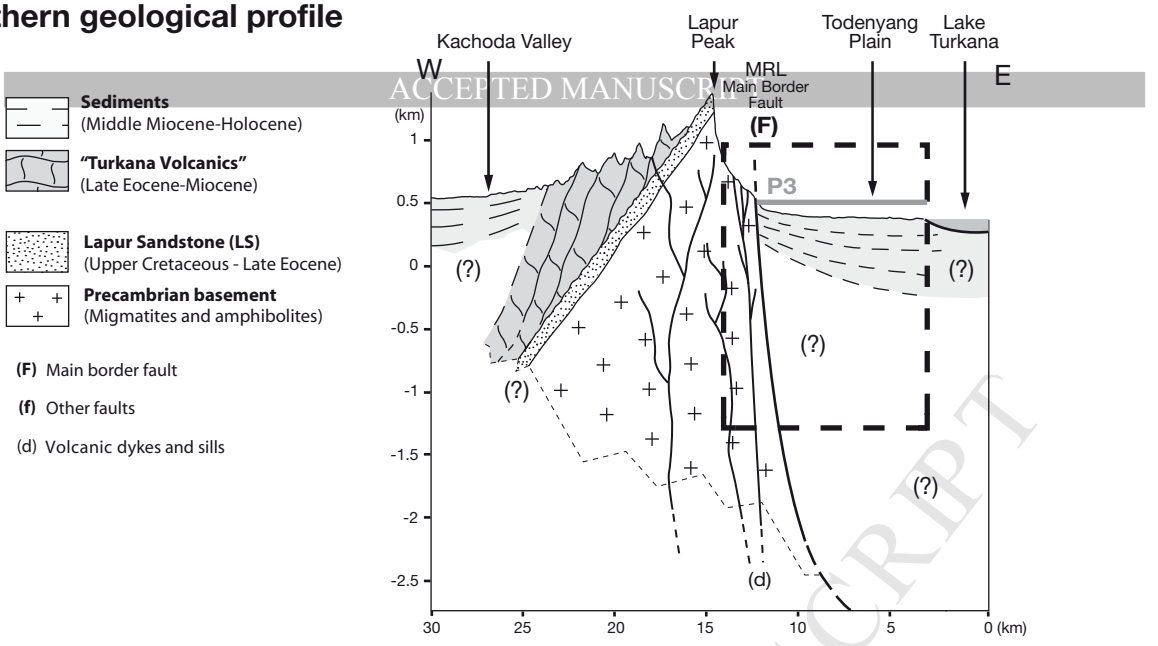

(b) Central geological profile

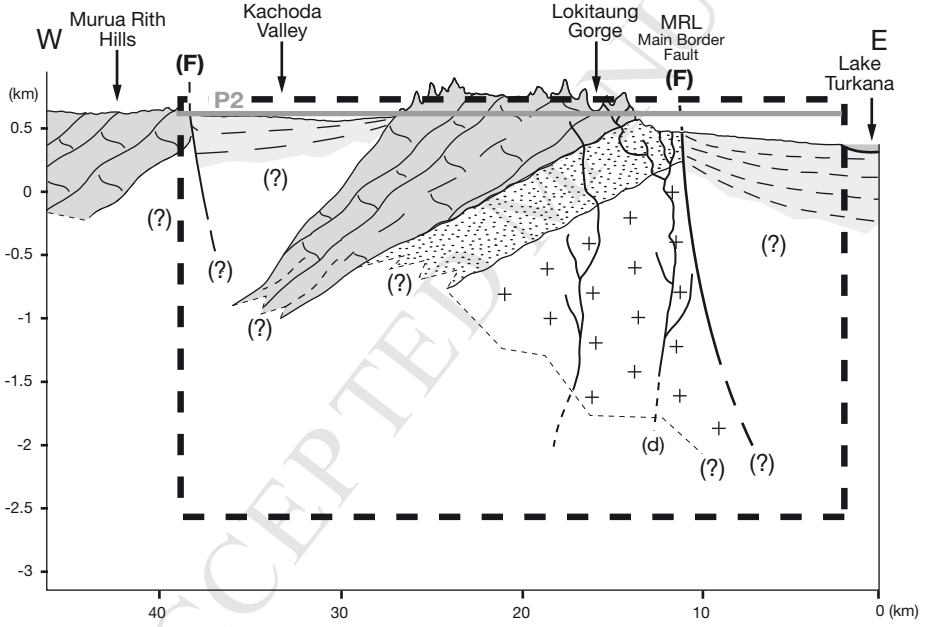

(c) Southern geological profile

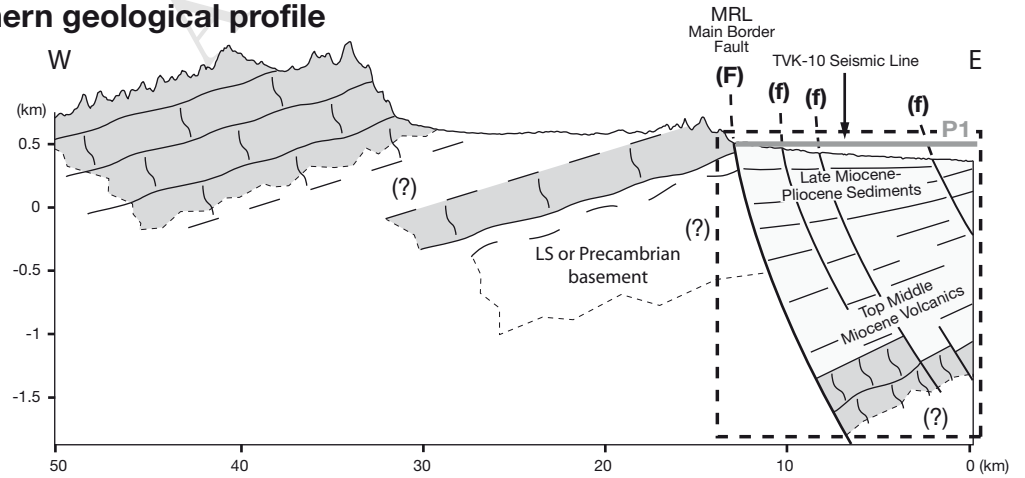

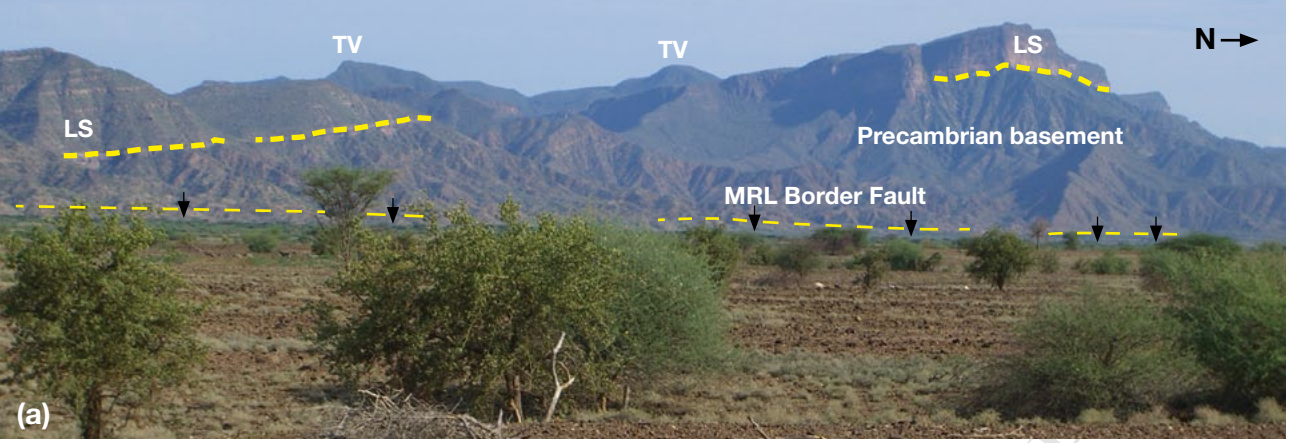
TV
TV
LS
N
LS
Precambrian basement
MRL Border Fault
(a)


(b)


(c)

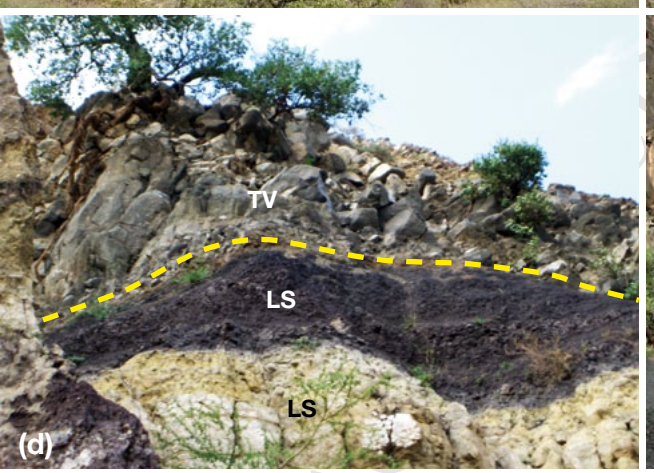
TV
LS
LS
(d)


(e)


(f)


(g)

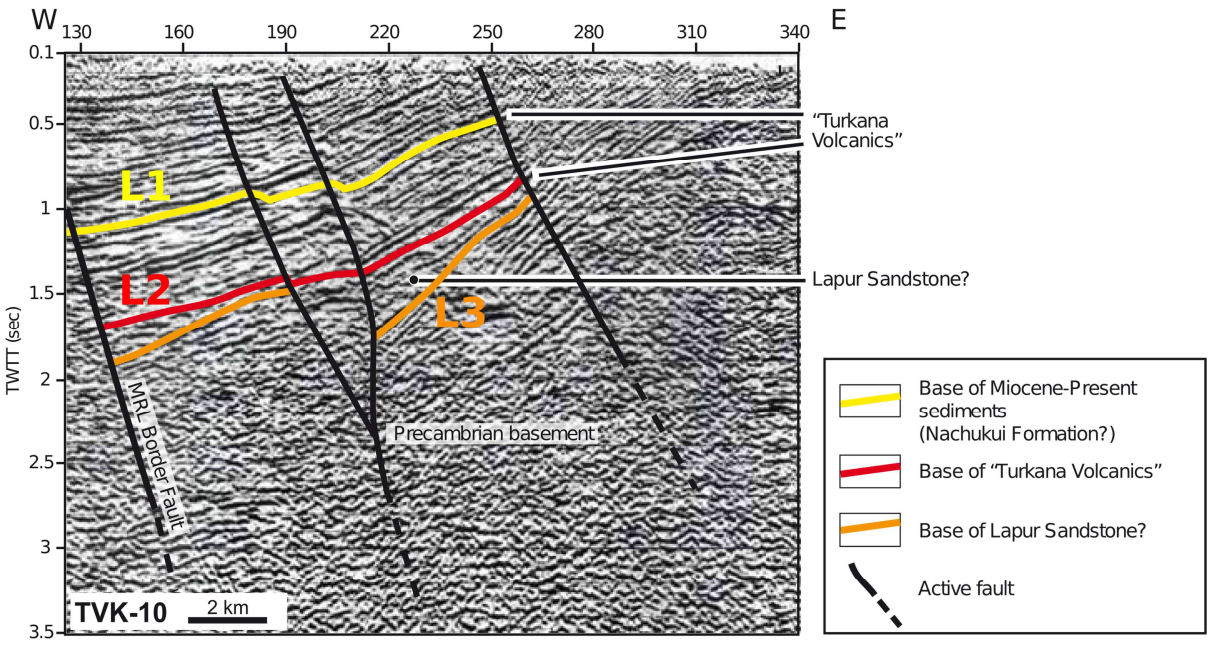


(a)


(b)


(c)


(d)


(ea)
(eb)

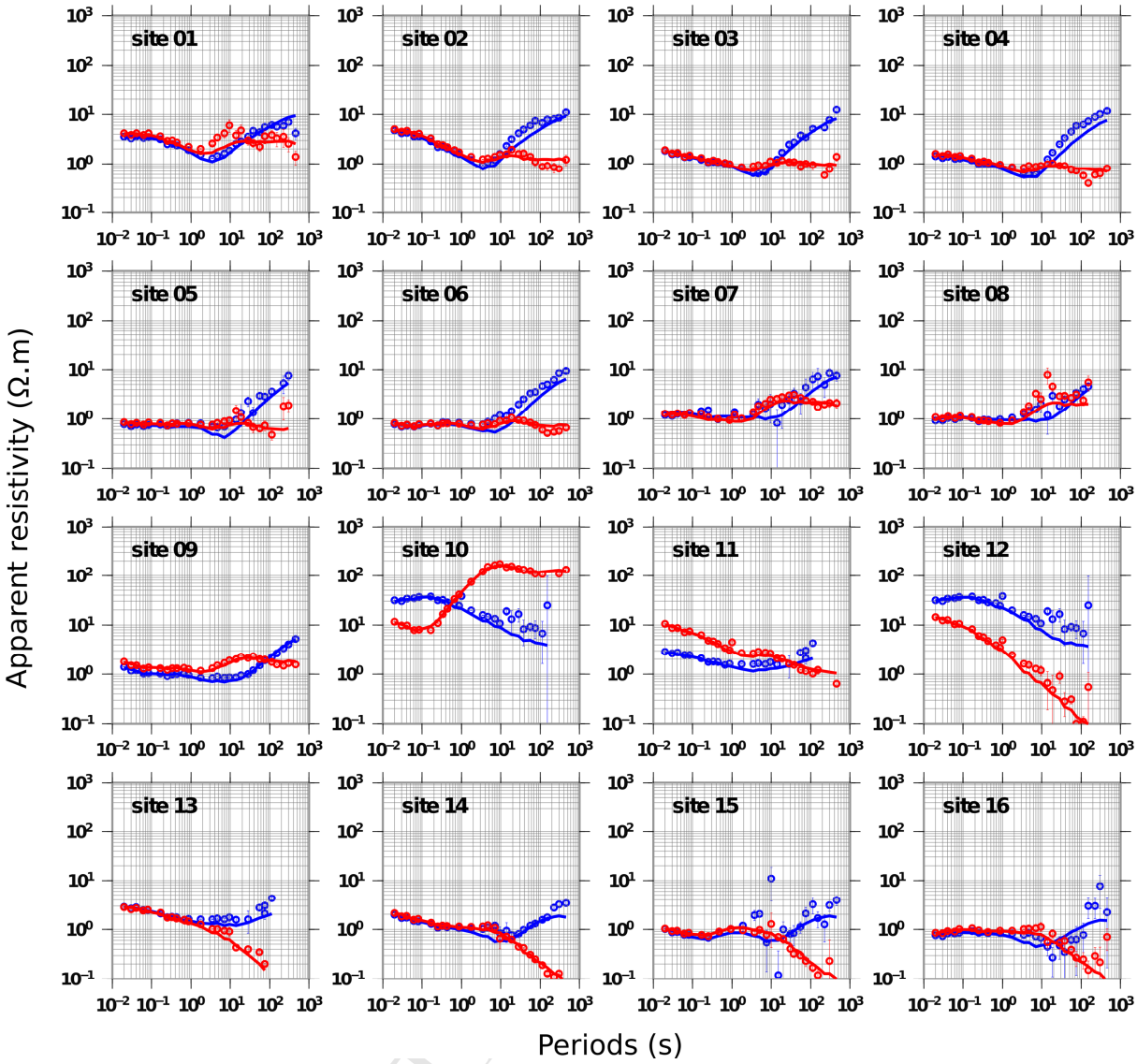

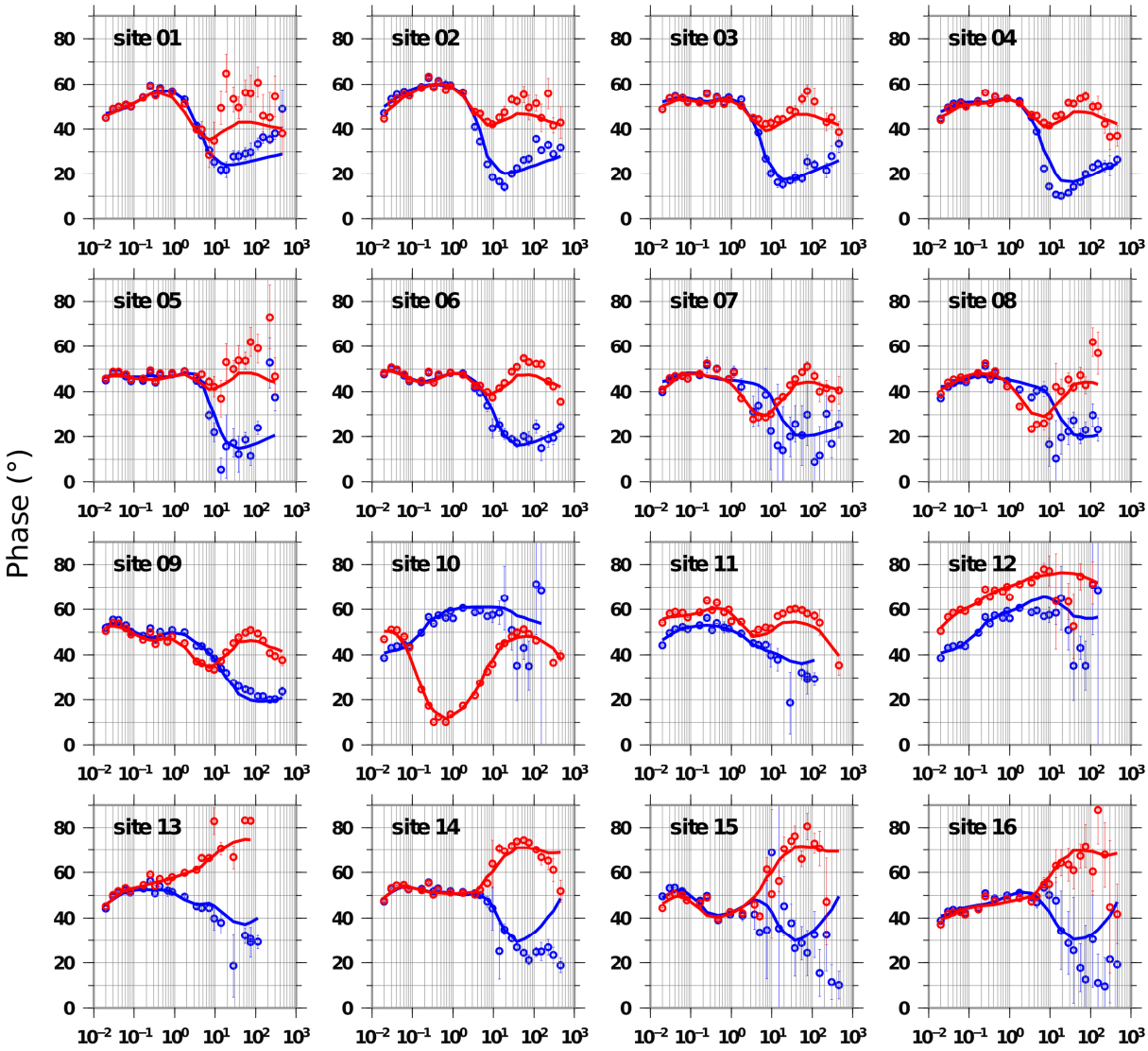

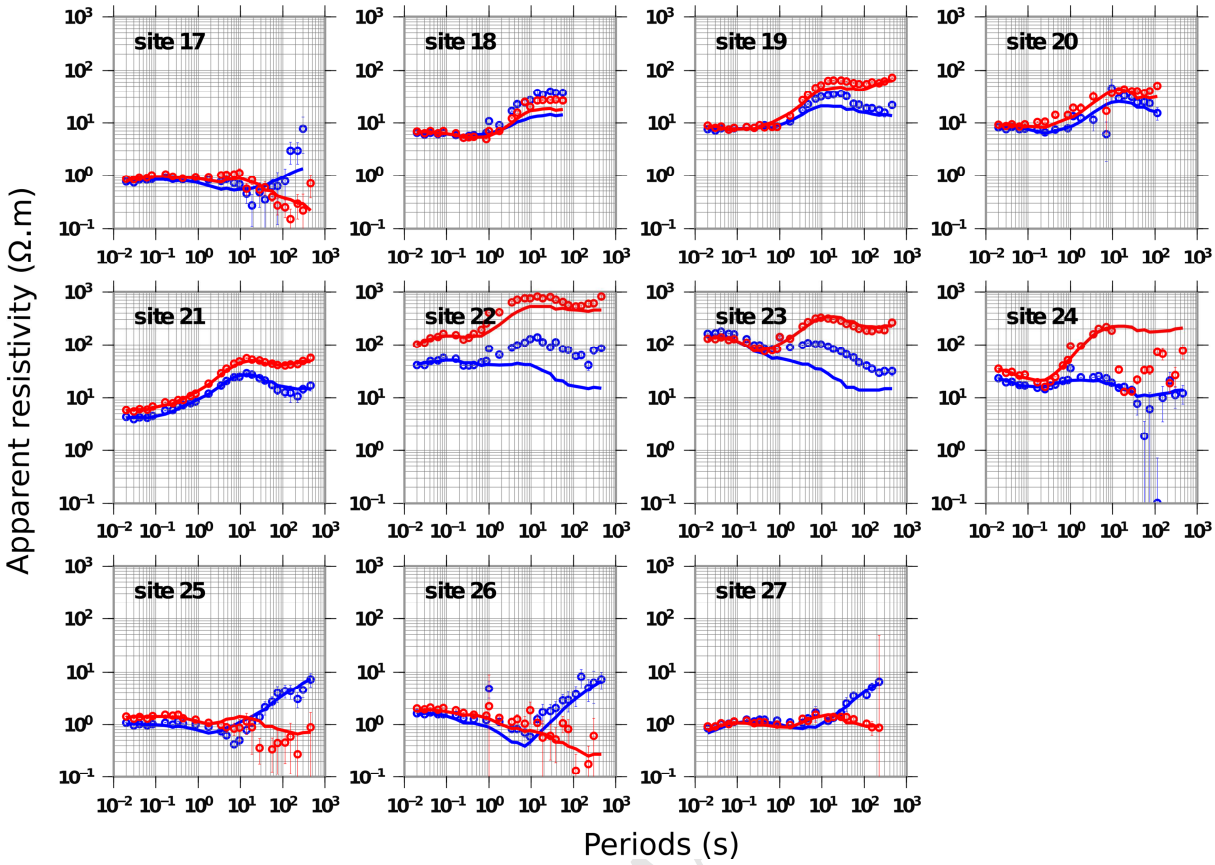

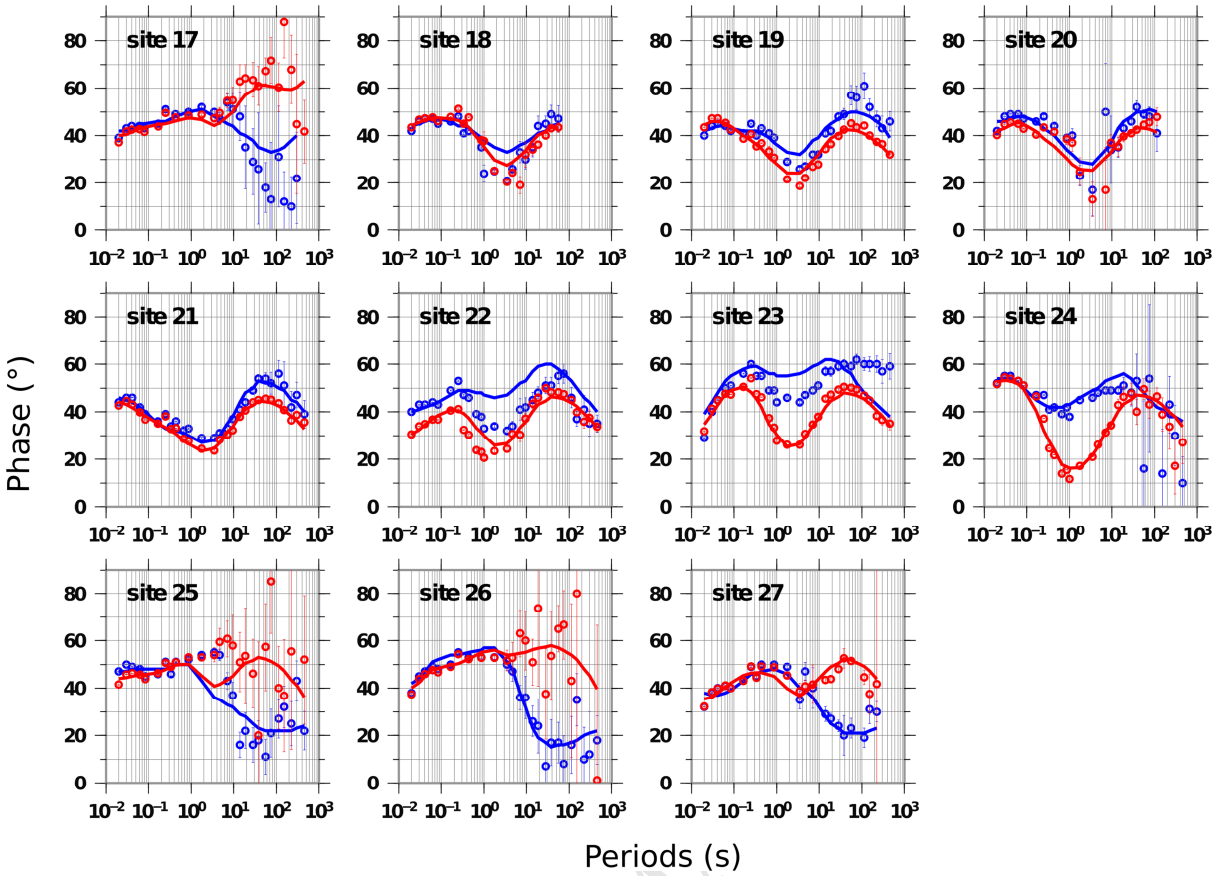

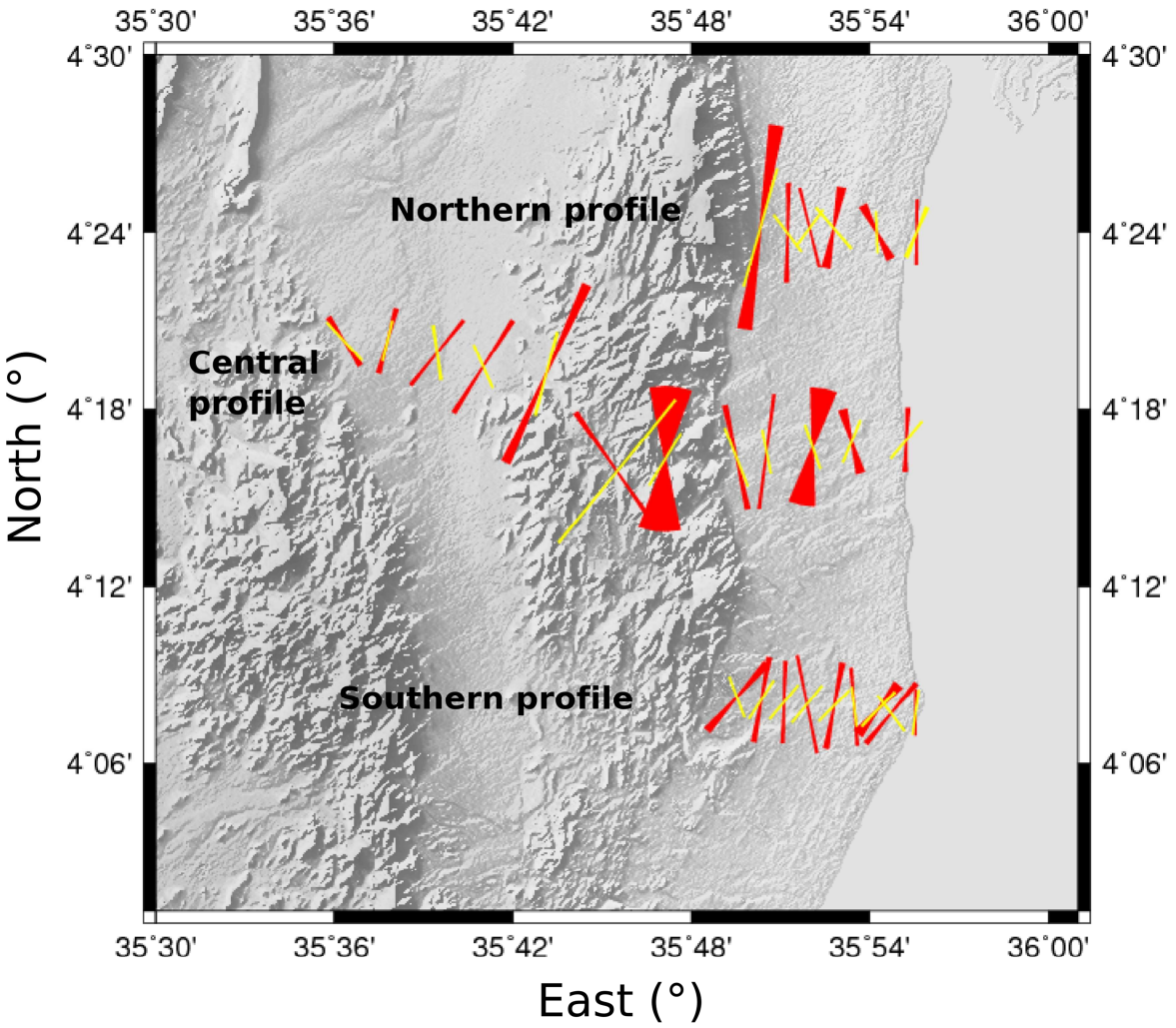

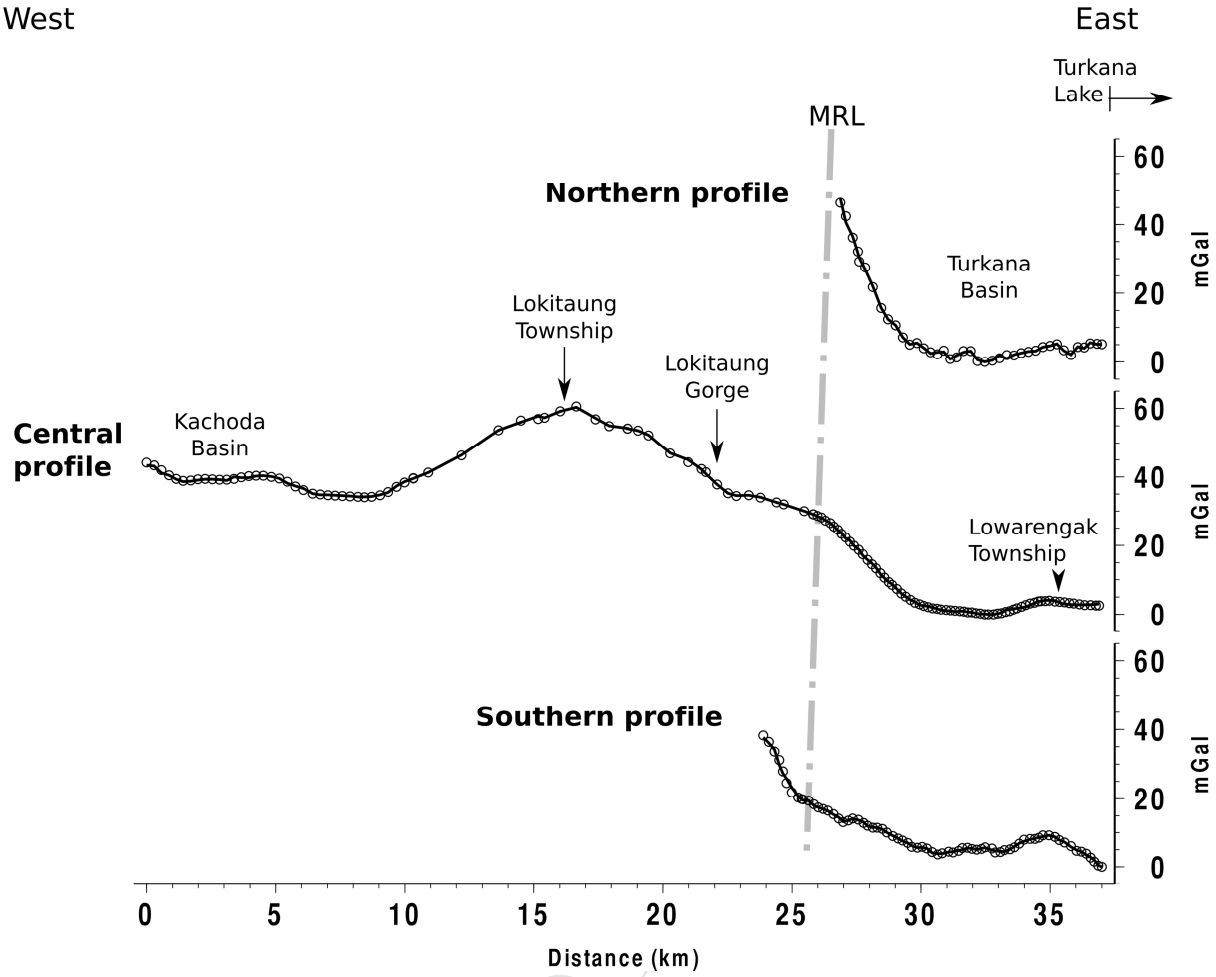

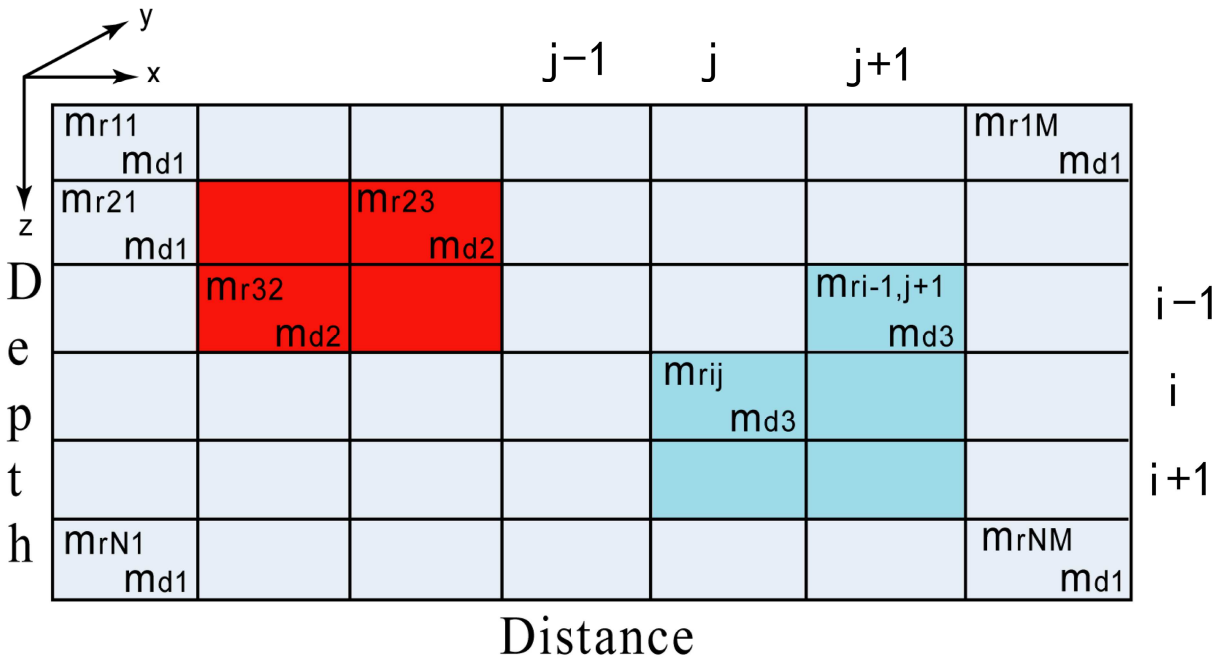

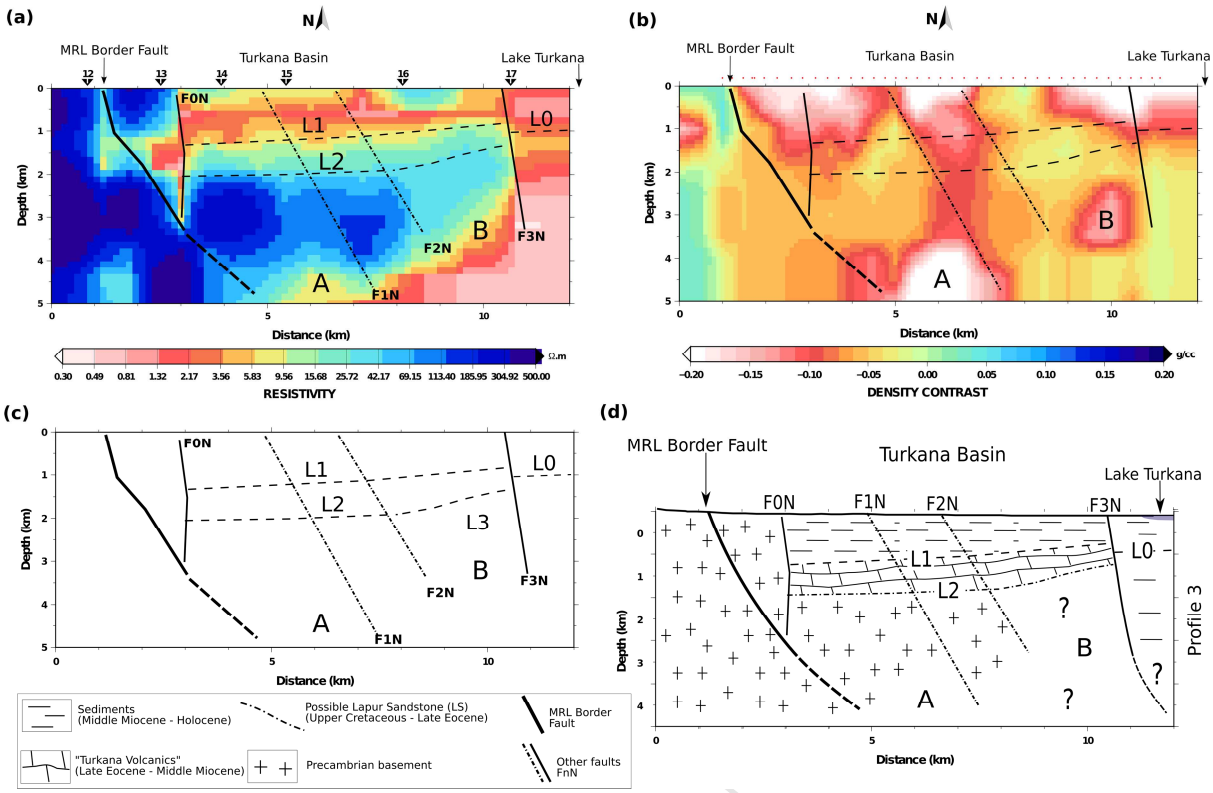

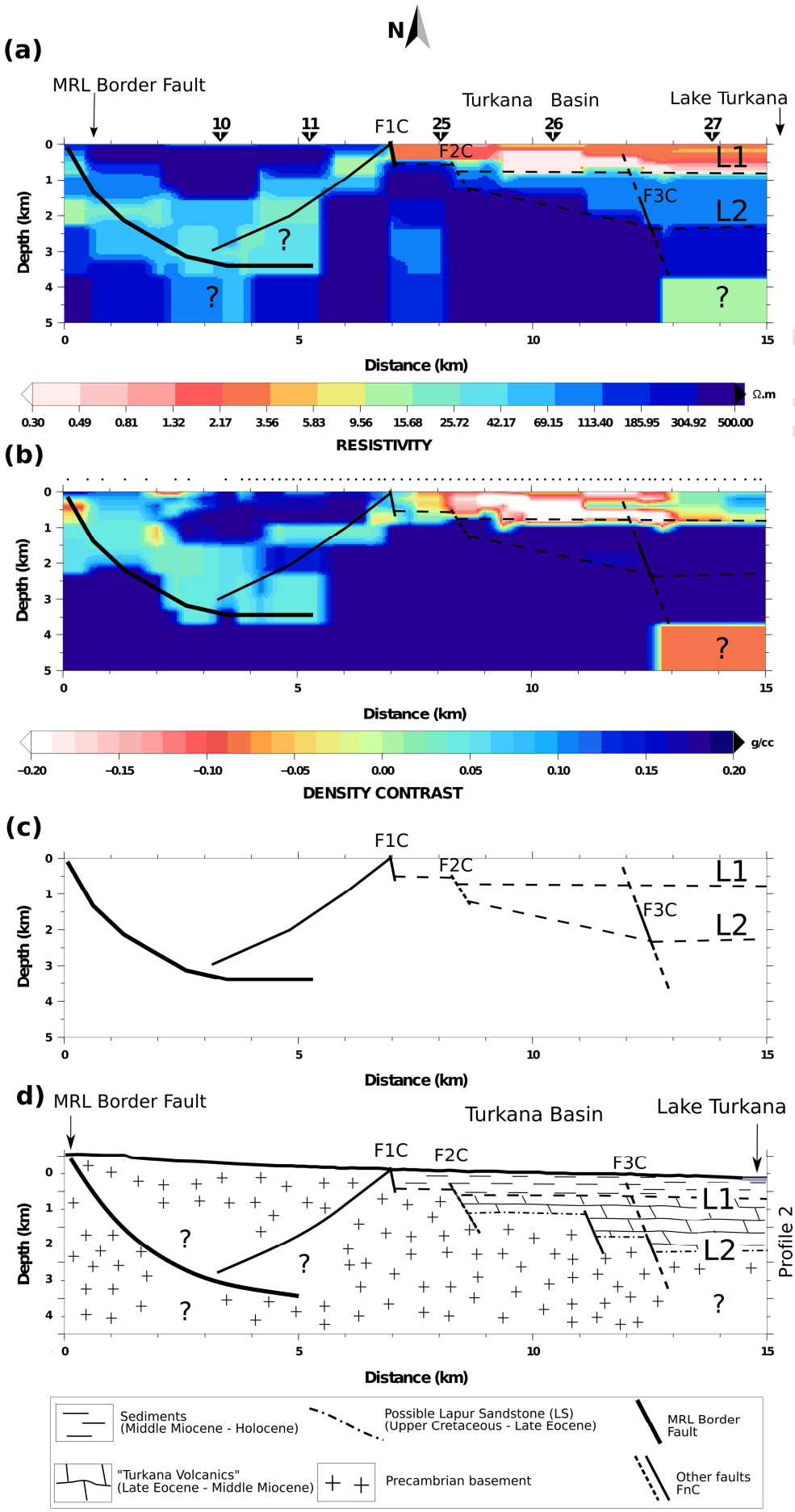
N
(a)
MRL Border Fault
Turkana Basin
Lake Turkana
10
11
F1C
25
F2C
26
27
L1
F3C
L2
?
?
?
Depth (km)
Distance (km)
Ω.m
0.30 0.49 0.81 1.32 2.17 3.56 5.83 9.56 15.68 25.72 42.17 69.15 113.40 185.95 304.92 500.00
RESISTIVITY
(b)
Depth (km)
Distance (km)
g/cc
−0.20 −0.15 −0.10 −0.05 0.00 0.05 0.10 0.15 0.20
DENSITY CONTRAST
(c)
F1C
F2C
L1
F3C
L2
Depth (km)
Distance (km)
d)
MRL Border Fault
Turkana Basin
Lake Turkana
F1C
F2C
F3C
L1
L2
?
?
?
?
Profile 2
Depth (km)
Distance (km)
Sediments
(Middle Miocene - Holocene)
Possible Lapur Sandstone (LS)
(Upper Cretaceous - Late Eocene)
MRL Border Fault
"Turkana Volcanics"
(Late Eocene - Middle Miocene)
Precambrian basement
Other faults
FnC

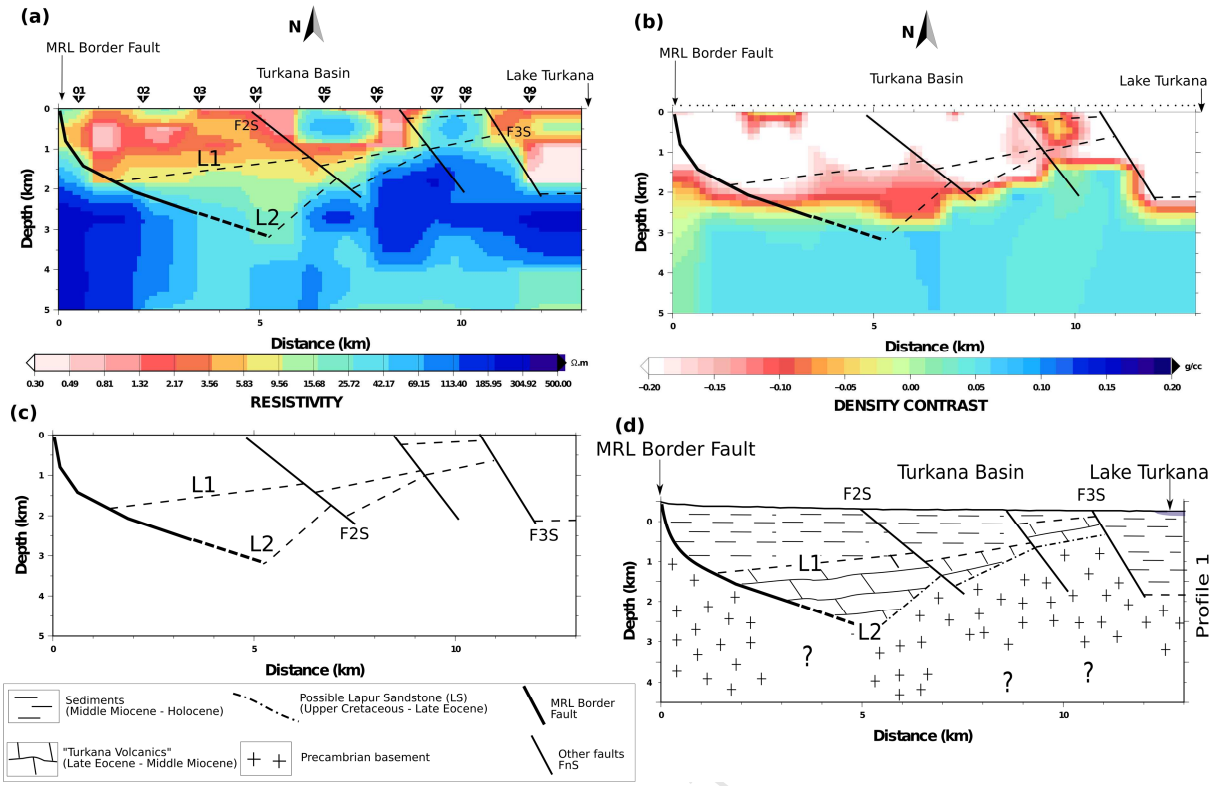

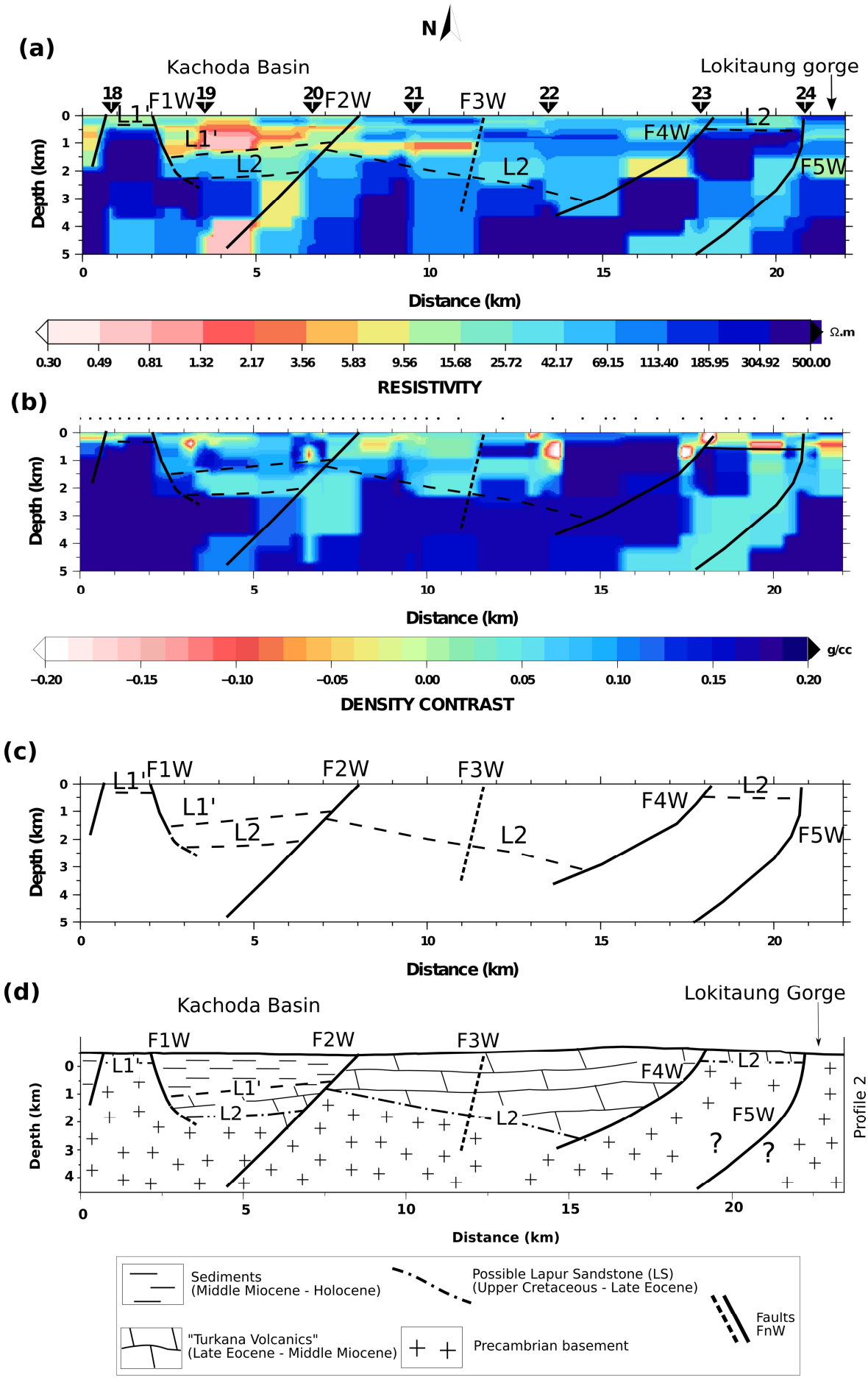
N
(a)
Kachoda Basin
Lokitaung gorge
18
19
20
21
22
23
24
F1W
F2W
F3W
F4W
F5W
L1'
L2
Depth (km)
Distance (km)
Ω.m
0.30
0.49
0.81
1.32
2.17
3.56
5.83
9.56
15.68
25.72
42.17
69.15
113.40
185.95
304.92
500.00
RESISTIVITY
(b)
g/cc
−0.20
−0.15
−0.10
−0.05
0.00
0.05
0.10
0.15
0.20
DENSITY CONTRAST
(c)
(d)
Profile 2
?
Sediments
(Middle Miocene - Holocene)
Possible Lapur Sandstone (LS)
(Upper Cretaceous - Late Eocene)
Faults
FnW
"Turkana Volcanics"
(Late Eocene - Middle Miocene)
Precambrian basement

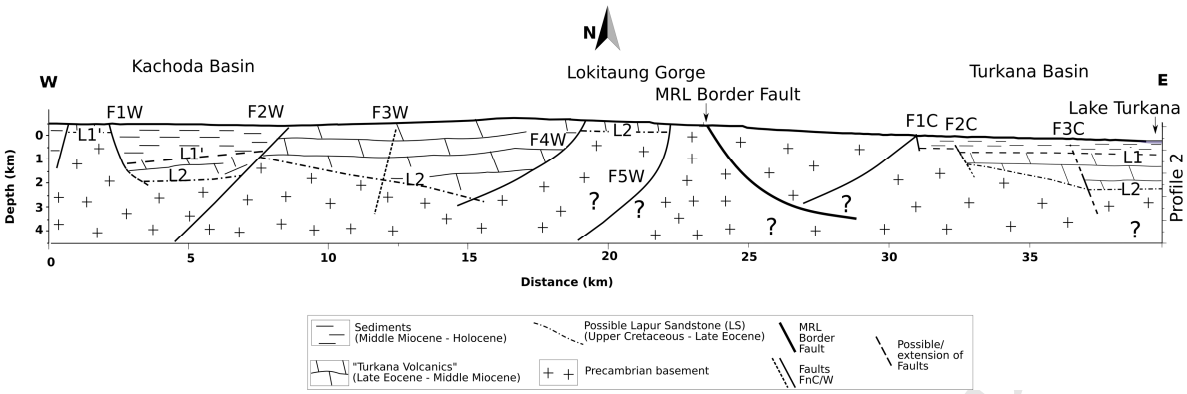

Highlights

1) Confirm the Turkana half-graben basins geometry and organization at depth.

2) Delineate the “Turkana Volcanics” unit as well as horizontal/vertical variations

3) Characterize the depth and topography of the basement in the Northwest Turkana and Kachoda basins.

4) Characterization of the new Kachoda half-graben basin, thickness of its sedimentary infill; presence and thickness of the Turkana Volcanics at depth units; uncertainty in terms of presence of the Lapur Sandstone at depth; variations of basement topography.

5) MT and gravity data used in Turkana to surpass the poor quality of seismic.